DOI: 10.1002/ejoc.200901340

Recent Advances in Stereodynamics and Conformational Analysis by Dynamic NMR and Theoretical Calculations

Daniele Casarini,[a] Lodovico Lunazzi,[b] and Andrea Mazzanti*[b]

Keywords: NMR spectroscopy / Density functional calculations / Conformation analysis / Atropisomerism / Molecular motions

Dynamic NMR spectroscopy can determine energy barriers due to internal motion over the range of about 4.5–23 kcal mol^{-1}. Conformational analysis of the frozen conformations can be simulated and interpreted by reliable theoretical calculations based mainly on density functional theory (DFT). The same calculations can identify transition states and predict the values of energy barriers involved in stereodynamic processes. This review describes recent advances in the experimental and theoretical approaches used in the field of the stereodynamic analysis, reporting a number of examples taken from the recent literature.

1. Introduction

Variable-temperature NMR spectroscopy, often referred to as dynamic NMR (DNMR), is a powerful tool for investigating stereodynamic processes. Separate (anisochronous) signals, observed at appropriate temperatures at which motion is slow on the NMR timescale, broaden on warming and eventually coalesce when the motion becomes fast on that timescale. By computer simulation of the band shape the rate constants (k values) can be derived over the temperature range over which this feature is detectable. In the case of conformational processes the rates are not dependent upon the concentration, and the corresponding k values usually cover a range of a few to a few thousand reciprocal seconds (s^{-1}). From the k values, free energies of activation ($\Delta G^{\neq}$ in kcal mol^{-1}) can be extracted by application of the Eyring equation, where T is the absolute temperature and k is the rate constant in s^{-1}; see Equation (1).

$$\Delta G^{\neq} = 4.574 \times 10^{-3} \cdot T \cdot [\mathrm{Log}_{10}(T/k) + 10.318] \quad (1)$$

This method allows $\Delta G^{\neq}$ values between about 4.5 and about 23 kcal mol^{-1} to be determined. The temperature ranges over which k values can be accurately measured by DNMR technique are usually quite small, however, so reliable values of $\Delta H^{\neq}$ and $\Delta S^{\neq}$ cannot normally be obtained. In the few conformational processes in which such accuracy has been achievable, the $\Delta S^{\neq}$ values were invariably found to be almost negligible within the experimental error, so $\Delta H^{\neq}$ appeared to be essentially equal to $\Delta G^{\neq}$. Reports of conformational processes that appear to show $\Delta S^{\neq}$ values substantially different from zero are most probably due to insufficiently accurate measurements.[1]

A number of books and reviews have previously been devoted to describing the applications of DNMR in conformational analysis.[2–14] Technical improvements in modern high-field NMR spectrometers have permitted previously unaccessible dynamic NMR investigations, so here we update earlier reviews by presenting a selection of DNMR studies from the last 10–15 years. This selection reflects the personal interests of the authors, so other excellent examples may not be reported in this microreview. The recent papers on stereodynamics reported here cover the most commonly occurring conformational processes in organic chemistry: ring inversion, restricted rotation and nitrogen inversion.

2. Experimental Methods

2.1 NMR Samples

Dynamic NMR often requires that spectra have to be recorded over a wide temperature range, ideally in the same solvent. For the high-temperature range, [D$_6$]DMSO (b.p. +210 °C) or [D$_2$]tetrachloroethane (b.p. +146 °C) are usually employed. Solvents without any hydrogen atoms, such as tetrachloroethylene (b.p. +121 °C), hexachloroacetone (b.p. +70 °C/6 mm Hg) or hexachlorobutadiene (b.p. +210 °C) are also used. Variable-temperature experiments down to –100 °C are usually recorded in CD_2Cl_2 (m.p. –97 °C), [D$_8$]THF (m.p. –118 °C) or CD_3OD (m.p. –95 °C). Quite a wide temperature range is accessible with [D$_8$]-toluene (from –95 °C to +110 °C).

[a] Department of Chemistry, University of Basilicata, via Nazario Sauro 85, 85100 Potenza, Italy
[b] Department of Organic Chemistry "A. Mangini", University of Bologna, Viale Risorgimento 4, 40136 Bologna, Italy
Fax: +39-051-2093654
E-mail: mazzand@ms.fci.unibo.it

Supporting information for this article is available on the WWW under http://dx.doi.org/10.1002/ejoc.200901340.

If the temperature has to be decreased well below –100 °C, the samples have to be prepared in a more sophisticated way, with use of liquefied gases such as Me_2O,[15] vinyl chloride,[16] propane,[17] propene,[18] Freons® or mixtures of these (see Table 1).

Table 1. Mixtures of solvents reported in the literature, together with the lowest attained temperatures.

Solvent mixture (v/v)	*T* [°C]	Ref.
$CHF_2Cl/CHFCl_2$, 3:1	–182	[22]
$CHF_2Cl/CHFCl_2$, 5:1	–190	[23]
$CHF_2Cl/CHFCl_2/CF_2Cl_2$, 3:1:1	–170	[24]
$CHF_2Cl/CHFCl_2/CHF_3$, 5:1:1	–188	[25]
$CHF_2Cl/CHFCl_2/CHF_3$, 3:1:1	–182	[26]
$CCl_2F_2/CBrF_3$, 4:1	–157	[27]
$CF_2Cl_2/CBrF_3$, 2:1	–166	[28]
$CHFCl_2/CCl_2F_2$, 1:1	–165	[29]
$CHF_2Cl/CHFCl_2$, 1:1	–174	[30]
$CHCl_2F/CH_2$=CHCl, 6:1	–160	[31]
Me_2O/THF, 3:1	–140	[32]
THF/Et_2O, 3:2	–135	[32]
$CHF_2Cl/CDFCl_2$, 3:1	–171	[33]
CH_2=CHCl/CS_2, 4:1	–131	[34]
CH_2=CHCl/CS_2, 3:2	–132	[34]
CH_2=CHCl/$CHFCl_2$, 5:2	–152	[35]
CD_2Cl_2/[D_8]toluene, 1:1	–120	[36]

The use of hydrogen-containing solvents is often impractical because of their very strong signals, which can overlap with the signals of the dilute solute. Freons®, in contrast, either do not show any signal in the proton spectra ($CBrF_3$, CF_2Cl_2), or only give a signal in the aromatic region of the spectrum ($CHFCl_2$, CHF_2Cl, CHF_3) and are also quite good solvents even at very low temperatures.[19] Moreover, the simple preparation of $CDFCl_2$ starting from $CDCl_3$[20] can also remove this signal and avoid the need for the use of any additional lock source.[21]

A quite popular combination used for dynamic NMR studies is a $CHF_2Cl/CHFCl_2$ mixture (ca. 3:1 v/v) with a small amount of a deuterated solvent (usually C_6D_6 or [D_6]-acetone) used for the lock signal. This mixture remains fluid down to about –180 °C. A second very useful combination, with similar characteristics, is a $CDF_2Cl/CHFCl_2$ mixture (ca. 2:1 v/v). If the ^{1}H NMR spectrum need to be monitored in the aromatic region, $CDFCl_2/CBrF_3$, $CF_2Cl_2/CBrF_3/C_6D_6$ or $CBrF_3/C_6D_6$ mixtures are usually good, the only limitation being the poor solvent capability of $CBrF_3$.

When solvents that are gaseous at ambient temperature are needed, the preparation of the samples requires the use of a vacuum line. The NMR tube (normally a high-quality borosilicate tube to which a Pyrex extension pipe has been fused) is filled with the required amount of the compound, and a small amount of C_6D_6 for locking purposes (about 0.05 mL) is then introduced by microsyringe. The NMR tube is then immersed in liquid nitrogen and evacuated, in order subsequently to condense about 0.65 mL of the gaseous solvents, which are transferred from lecture bottles connected to the vacuum line. The tube is finally sealed under reduced pressure (0.001 bar) with the aid of a methane/oxygen torch. In order to avoid rapid temperature changes, the sample is allowed to warm slowly to ambient temperature, at which Freons® develop pressures that depend on the type of mixture employed (about 15 bars in the case of $CBrF_3$, for instance).

For reasons of safety the sample is stored for many hours at ambient temperature so that it can then be safely introduced into the probe head of the spectrometer, previously cooled to about –30 °C to avoid any risk.

When the NMR spectrometer is operated at very low temperature, a flow of very dry, pure nitrogen is first passed through a pre-cooling unit adjusted to –50 °C, and the nitrogen then enters into an inox-steel heat-exchanger im-

Daniele Casarini was born in 1955. He obtained his doctoral degree in 1979 in Industrial Chemistry at the University of Bologna under the guidance of Professor A. Fava. He has worked in the pharmaceutical industry specializing in synthesis and chiral resolution. In 1983 he started his research career and joined Professor Lunazzi's group. During a sabbatical leave in 1990 he joined Professor R. K. Harris's group at the University of Durham (UK), where he gained knowledge in the area of the NMR in the solid state. Since 1998 he has been working as associated professor of Organic Chemistry at the University of Basilicata (Italy). His research mainly focuses on the synthesis and conformational analysis studies of organic molecules and has resulted in over than 80 papers relating to conformational studies by dynamic NMR spectroscopy.

Lodovico Lunazzi was born in 1940 and graduated in Industrial Chemistry at the University of Bologna in 1963. He was a postdoctoral fellow (1967–1968) at the National Research Council (Ottawa, Canada) with S. K. Brownstein, a visiting professor at the Universities of Grenoble (France) and Nijmegen (The Netherlands) and a visiting scientist at NRC, Ottawa. Since 1975 he has been professor of Organic Chemistry at the University of Bologna. He is the recipient of the Gold Medal of the Italian Chemical Society for Magnetic Resonance and of the "Mangini" medal for Physical Organic Chemistry and is a co-author of 250 papers on the application of ESR and NMR spectroscopy to organic chemistry.

Andrea Mazzanti was born in 1970. He graduated in Industrial Chemistry at the University of Bologna in 1994. In 1997 he worked at University College London (UK) with Professor J. E. Anderson. He received his Ph.D in Chemical Science (dynamic NMR of hindered carbinols) under the supervision of Professor L. Lunazzi in 1999. Since 2001 he has been a research assistant in the Department of Organic Chemistry at the University of Bologna. In 2004 he was awarded the Italian Chemical Society "Ciamician" medal for young organic chemists. His research is focused on the use of dynamic NMR spectroscopy in combination with DFT calculations for the study of dynamic processes and conformational chirality of organic molecules. He is a co-author of about 100 papers relating to the use of NMR spectroscopy and theoretical calculations in organic chemistry.

mersed in liquid nitrogen and connected to the NMR probe head by a short vacuum-insulated transfer line. Gas flows of 10–40 L min^{-1} are required in order to descend to the desired temperature. All the cold parts of the equipment must be insulated with neoprene foam.

2.2 Temperature Measurement

The determination of the exact temperature inside the sample is crucial for the determination of the thermodynamic parameters. An error of ±2 °C in the temperature causes an error in $\Delta G^{\neq}$ of 0.1_5 to 0.2 kcal mol^{-1},[37] and this is usually the main source of errors in the DNMR technique. A spectrometer shows a "dial temperature", determined by a thermocouple underneath the NMR tube. The temperature of the sample giving rise to the observed NMR signals (i.e., in the region of the RF coils) is usually different, and can be correlated to the "dial temperature" by calibration. Such calibration of the spectrometer probe can be performed with a digital thermometer and a Cu/Ni thermocouple[38] placed in an NMR tube filled with an appropriate solvent (usually isopentane for the low-temperature range and DMSO for the high-temperature range). This sample is inserted into the spectrometer and the conditions are kept as close as possible to those used in the subsequent measurements. In particular, the sample is not spun and the gas flow is the same as that used during the acquisition of the spectra. From the experimentally measured temperatures and dial temperatures, a calibration curve can be derived, but it should occasionally be recalibrated. The uncertainty in temperature measurements with such a calibration curve can be estimated as ±2 °C.

2.3 Line Shape Simulation

The rate constants involved in conformation processes detectable by dynamic NMR cover approximately the range from 10^0 to 10^6 s^{-1}. When two nuclei A and B are exchanged in a dynamic process with a kinetic constant k, the corresponding lines broaden, reach the coalescence point and eventually yield an average signal when the exchange rate constant becomes large. The presence of more than two signals and of more than a single rate constant can complicate this situation; nevertheless the whole system can be mathematically simulated. With the use of increasing calculation power it is possible to handle mathematical models that can simulate second-order spectra and quite complex spin systems (up to 11 nuclei).[39] Once a good spectral simulation is obtained at the temperature at which all the dynamic processes are frozen (i.e., when $k = 0$), the line shape at higher temperatures can be simulated by changing the values of the rate constants. Corrections are needed if chemical shifts, J couplings and conformer ratios are also temperature-dependent. Through matching of simulated and experimentally measured spectra, the kinetic constant (k value) is obtained at each given temperature and the free energy of activation ($\Delta G^{\neq}$) can then be derived by means of Equation (1), above. An example of how quite a complex spectral pattern[40] can be reproduced is displayed in Figure 1.

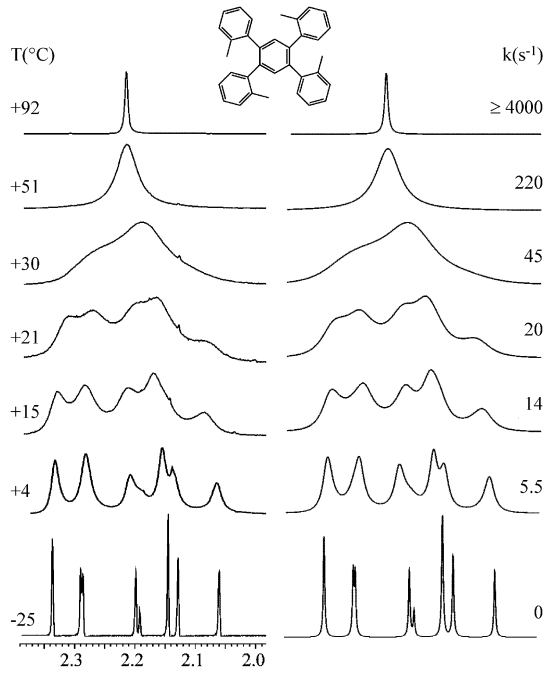

Figure 1. Left: temperature dependence of the eight ^{1}H NMR methyl signals due to the five unequally populated conformers of 1,2,4,5-tetra(*o*-tolyl)benzene in $CDCl_2CDCl_2$ at 600 MHz. Right: line shape simulation obtained with the rate constants indicated. (Reprinted with permission from *J. Org. Chem.* **2005**, *70*, 10062–10066. Copyright 2005, American Chemical Society).

3. Theoretical Approach

"It is a truism that in the past decade density functional theory has made its way from a peripheral position in quantum chemistry to center stage".[41]

Up to the end of the 1990s, conformational calculations of organic molecules were mainly performed by molecular mechanics (e.g., MM3,[42] MMX,[43] MMFF,[44] Amber[45] etc.) and semiempirical methods (AM1,[46] PM3,[47] MINDO[48] being the most popular). These calculations were reasonably simple and could be completed in short times on standard desktop PCs without the need for supercomputers.[49] The results obtained were often quite accurate, at least for the calculation of the ground-state conformations. For the calculation of transition states, in contrast, these methods have intrinsic limitations. Usually the interconversion barriers were calculated by moving the relative parts of the molecule in fixed steps and optimizing the remaining parts. Otherwise, a "handmade" transition state was assumed, and the geometry was optimised within certain constraints. As a result of these approximations, the computed barriers were prone to relatively large errors, and there was no guarantee that a real transition state had been located.

When the application of ab initio methods (HF) became available for medium-sized molecules the situation was greatly improved, although the neglecting of electron correlation was a serious limitation, partially solvable only through the employment of higher methods such as MP2.[50] Unfortunately, this approach was not manageable without a very large computational facility.

Density Functional Theory (DFT) has the great advantage of taking account of electronic correlation at a reasonable computational cost.[51] In recent years, the availability of inexpensive high-performance servers[52] and manageable software (Gaussian 03,[53] Turbomole,[54] Spartan[55] and NWChem[56] being the most famous) has allowed high-level calculations to be performed in a reasonable amount of time for molecules containing up to 50–60 atoms.

DFT calculations are very interesting for dynamic NMR because they can be applied both to obtain the conformations of ground states and also to find the correct geometries and energies of transition states. Thanks to vibrational analysis, there is *always* confirmation that the correct transition state has been unambiguously identified. There are, however, some particularities in the use of these calculations in conformational analysis that are worth considering.

3.1 Ground States

Some uncertainty is involved in determining the relative energies of possible ground states. In recent years many papers addressing the performance of various DFT functionals in determining relative energies in reactions have appeared,[57] but for conformational analysis there have been very few.

Our experience is that the very popular B3LYP functional,[58] based on the relatively small 6-31G(d) or the larger 6-311++G(2d,p) basis sets, is usually a very good compromise between accuracy and computational cost. The geometries obtained by calculations can in many cases be checked by X-ray diffraction data, and the relative energies of conformations can be compared with the results of variable-temperature NMR spectroscopy. Although such a calculation usually refers to an isolated molecule, whereas X-ray studies reflect the solid state and NMR results are for solutions, DFT structures compare very well with experimental observations in almost all cases, and the relative energies of possible conformations are correctly calculated.

3.2 Transition States

The determination of transition state structures and energies is a crucial point for dynamic analysis, because correct simulation of energy barriers could greatly help understanding of the dynamic process detected by dynamic NMR spectroscopy. As addressed by D. Young,[59] a transition state (or saddle point) structure is mathematically defined as "the geometry that has zero derivative of energy with respect to moving every one of the nuclei, and has positive second derivative energy for all but one geometric movement". In other words, a transition state linking two energy minima represents a maximum of energy in the direction of the reaction path, but it is a minimum in all other directions.

There are several algorithms that can be used to find a transition structure; all invariably start by calculating the matrix of second derivatives of energy with respect to nuclear motion (Hessian matrix). The nuclei are then moved with the goals of increasing the energy in the directions corresponding to negative values of the Hessian and of lowering the energy in the directions corresponding to positive values. One of the most widely used methods, the Berny algorithm, follows the quasi-Newton approach, which assumes a quadratic shape of the potential energy surface (PES). Therefore, the optimisation is able to find the transition state only if the starting geometry is sufficiently close to that of the transition state.

Once a stationary point is found, the primary way to verify whether it corresponds to a transition state is to compute the vibrational frequencies. A transition state must have only one negative (i.e., imaginary) frequency, and the vibrational motion associated with this frequency corresponds to the motion going towards reagents in one direction, and towards the products in the other. Many molecular modelling packages (Gaussview,[60] Molden[61] and others) allow one to visualise an animation of the molecular displacements corresponding to the calculated frequencies, clarifying whether the correct transition state has been found.

Unfortunately, in contrast with the transition states for high-energy processes (such as those involved in a chemical reaction), in which the imaginary frequency usually has a large value, transition states involved in internal dynamic processes usually display small negative vibrational frequencies and can therefore be difficult to locate, especially in the presence of other possible internal motions. On the other hand, the geometry of a transition state is much simpler to idealise, because many geometrical parameters are fixed by the molecular scaffold.

3.3 Thermodynamic Corrections

The total energy computed by a geometry optimisation corresponds to the minimum on the potential energy curve. To compare data from calculations with experimentally measured values, thermodynamic corrections are usually required. In particular, the calculation of the zero-point energy and the thermodynamic corrections are usually printed out by the software after the vibrational analysis phase. In our recent experience, however, we have noted that in most cases the total energies themselves give the best fits with experimentally acquired DNMR spectroscopic data, and for this reason the reported energies are usually not corrected for zero-point energy contributions or other thermodynamic parameters. This approach cushions artefacts that might result from the inevitably ambiguous choice of a suitable reference temperature, from empirical scaling factors

(tuned for a set of small molecules)[62] and from the idealisation of low-frequency vibrators as harmonic oscillators (particularly important in cases of internal motions, for which a lot of the calculated frequencies fall below 500–600 cm^{-1}).[63] Table 2 gives examples of the very good agreement that can be achieved between DFT-computed and experimentally measured dynamic NMR values in the case of the aryl–aryl rotation barriers in *ortho*-substituted biphenyl derivatives.[64]

Table 2. Computed (DFT) and experimentally measured (DNMR) Ar–Ar rotation barriers (in kcal mol^{-1}) of some *ortho*-substituted biphenyls (the *meta* substituent Y is needed as a diastereotopicity probe for the DNMR experiments).

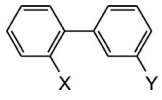

X	Computed	Experimentally measured
N^+Me_3[a]	18.2	18.1
*t*Bu[a]	15.6	15.5
*i*Pr[b]	11.1	11.1
I[a]	9.9	10.0
Br[a]	8.5	8.7
NH_2	8.4	8.1
NO_2	7.8	7.6
Cl[b]	7.3	7.7
Me[b]	7.1	7.4
NMe_2[a]	6.8	6.9
OMe[a]	4.5	5.6

[a] Y = $SiMe_2$*i*Pr. [b] Y = *i*Pr.

It also has to be noted that DFT calculations can reliably calculate chemical shifts, as reported in recent literature.[65] In the field of dynamic NMR and conformational analysis the calculation of chemical shifts and *J* couplings can be helpful in selecting from various possible ground state conformations. The accuracies of the calculations are usually very good because these conformations are frozen at low temperatures, so averaging of the calculated shifts to account for internal motions is not necessary.

4. Case Studies

4.1 Ring Inversion

Many DNMR-based studies relating to the inversion of a variety of rings, particularly derivatives of cyclohexane, have been reported.[12–14] Accurate investigations of larger rings (Scheme 1), which yield more complex spectra, have been reported in the last few years, owing to the availability of more sophisticated NMR hardware, together with the opportunity to approach these problems with the help of molecular mechanics and, more recently, of reliable DFT computations.

The ^{13}C NMR spectrum of *trans*-cyclodecene (**1**),[66] for instance, shows that at –155 °C the single line corresponding to the ethylenic carbons splits into eight lines of different intensities, owing to the presence of five conformers

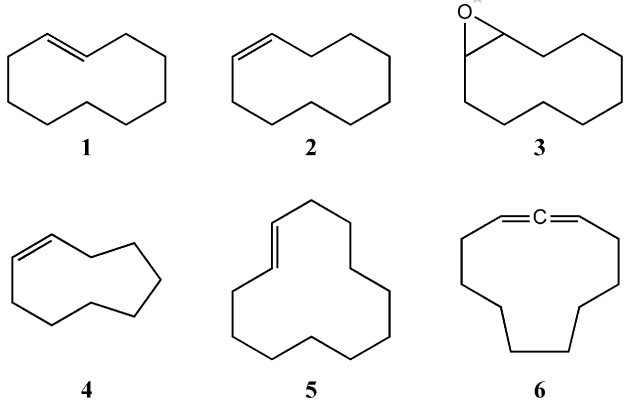

Scheme 1.

with populations ranging from 3% to 37.6% (Figure 2). Three of these conformers have C_1 symmetry and two have C_2 symmetry: they interconvert with a barrier of 6.5–6.6 kcal mol^{-1}.

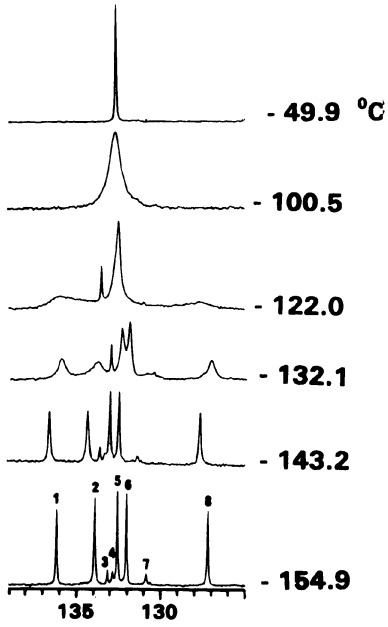

Figure 2. Low-temperature ^{13}C NMR spectra of the ethylenic region of **1** (75.6 MHz). (Reprinted with permission from *J. Am. Chem. Soc.* **1996**, *118*, 12821–12825. Copyright 1996, American Chemical Society).

Computations indicate that there are indeed five conformers with energies lower than all the other possible conformers, although three are predicted to display C_2 symmetry and two C_1 symmetry, which is the reverse of the experimental observation. For this reason a complete assignment of all these conformers could not be unambiguously achieved.

Unlike its *trans* isomer, *cis*-cyclodecene (**2**) adopts a single preferred conformation with a C_1 symmetry.[18] This is demonstrated by the ^{13}C NMR spectrum of the four pairs of methylene carbons, which at –143 °C split their four lines into 1:1 pairs (Figure 3).

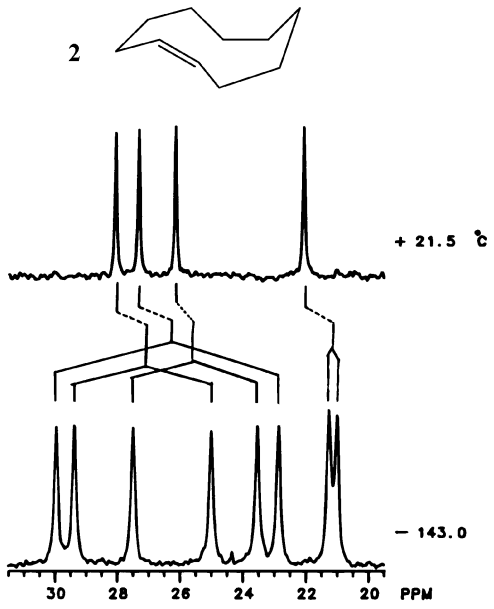

Figure 3. Correlation of room-temperature and slow-exchange ^{13}C NMR shifts (75.6 MHz) for the methylene carbons of *cis*-cyclodecene (**2**) in CF_2Cl_2. (Adapted with permission from *J. Am. Chem. Soc.* **1998**, *120*, 5312–5314. Copyright 1998, American Chemical Society).

Likewise split into a 1:1 pair is the ^{13}C NMR line corresponding to the two equivalent ethylene carbons. Such a feature is compatible with the C_1 symmetry of the computed conformer of lowest energy. There are two interconversion barriers involved in the stereodynamics of *cis*-cyclodecene: that derived from the ^{13}C NMR spectrum (6.6 kcal mol^{-1}) and that derived from the ^1H NMR spectrum of the ethylenic hydrogen atoms (10.9 kcal mol^{-1}). The stereodynamic pathways involved in these processes, however, were not discussed.

The corresponding epoxide **3** also adopts an analogous conformation, as shown by the ^{13}C NMR spectrum at –153 °C, in which the five lines corresponding to its carbons all split into 1:1 pairs, with the barrier involved in the interconversion process being 7.4 kcal mol^{-1}.

The epoxide of a smaller ring system, cyclohexene oxide,[25] was also found to adopt a single asymmetric conformation in that at –188 °C one of the three lines, due to the three pairs of carbons, splits into two (1:1 intensity ratio). This observation is compatible with the presence of a half-chair conformation, computed to have the lowest energy, interconverting between two enantiomeric forms. The experimental barrier for this ring-inversion process was measured as 4.3 kcal mol^{-1}. In the solid state the CP MAS ^{13}C NMR spectrum displays the analogous splitting of all three lines at a much higher temperature (–83 °C),[67] indicating that the barrier for this process is definitely higher in the crystalline state than in solution.

The single line corresponding to the ethylenic carbons in the ^{13}C NMR spectrum of *cis*-cyclononene (**4**) splits into three lines (Figure 4) at –189 °C.[17d] These lines were interpreted as due to the presence of two conformers, with the major one (66%) having C_1 symmetry and the minor one C_s symmetry.

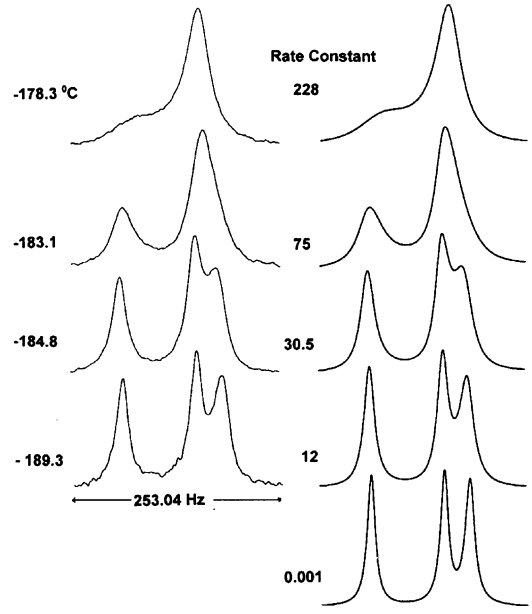

Figure 4. Experimentally observed (left) and calculated (right) NMR spectra of the olefinic carbons of *cis*-cyclononene (**4**) (75.6 MHz). The reported rate constants are in s^{-1}. (Reprinted with permission from *J. Org. Chem.* **1999**, *64*, 2418–2421. Copyright 1999, American Chemical Society).

Analysis of the CH_2 signals at this temperature also agrees with this interpretation. The C_s symmetry of the minor conformer, however, could possibly be the result of a time-averaged symmetry due to a motion still fast even at such a low temperature. The barrier involved in the exchanges of the two conformers was found to be equal to 4.3 kcal mol^{-1} and it was ascertained that the interconversion of sites in the major conformer takes place through conversion in the minor conformer. Calculations also suggest that the structures of the major and minor conformers are probably those indicated as **4a** and **4b** in Figure 5.

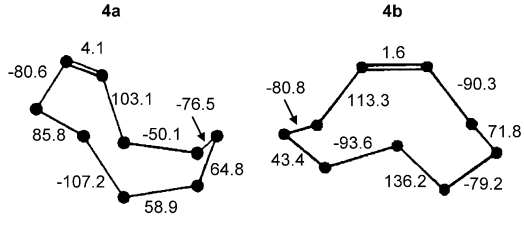

Figure 5. Computed (MM3) lowest-energy conformations of *cis*-cyclononene (**4**). CCCC dihedral angles are also shown. (Adapted with permission from *J. Org. Chem.* **1999**, *64*, 2418–2421. Copyright 1999, American Chemical Society).

A second dynamic process, with a higher barrier (8.0 kcal mol^{-1}), was also detected for **4** in the –125 to –100 °C range through monitoring of ^1H NMR spectra of

the CH_2 hydrogen atoms. It was suggested that such a process is a consequence of the exchange of the geminal hydrogen positions.

The single ^{13}C NMR line corresponding to the ethylenic carbons of *trans*-cyclododecene (**5**) broadens on cooling and at –164 °C eventually splits into seven lines.[68] These lines were interpreted as due to four conformers: three with C_1 symmetry (populations 57.0, 18.6 and 4.3%) and one (20.1%) with C_2 symmetry. This interpretation was broadly compatible with the 35 signals expected for the CH_2 region at the same temperature. A tentative attribution based on calculated energies and calculated ^{13}C shifts was proposed; structures **5a**, **5b** and **5d** were assigned to the conformers exhibiting C_1 symmetry and **5h** to that exhibiting C_2 symmetry (Figure 6).

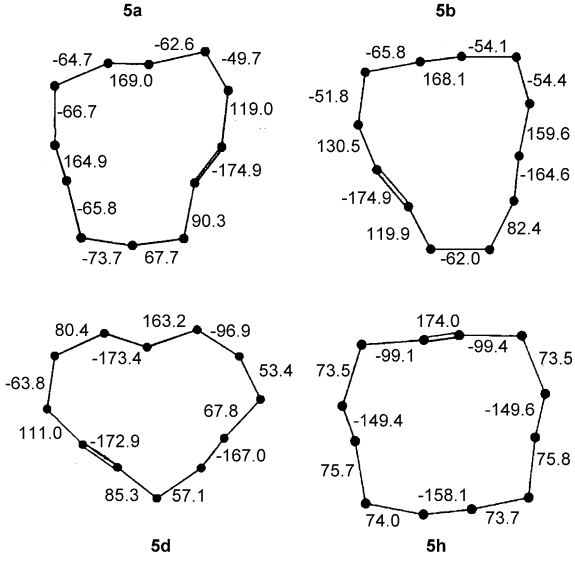

Figure 6. The four computed (MM3) lowest-energy conformations of *cis*-cyclododecene (**5**). CCCC dihedral angles are also shown. (Adapted with permission from *J. Org. Chem.* **1999**, *64*, 4580–4585. Copyright 1999, American Chemical Society).

The six ^{13}C lines of cycloundeca-1,2-diene (**6**) broaden on cooling and split into 17 lines at –166 °C (Figure 7). This feature was attributed to a minor (46.5%) conformation with C_1 symmetry exhibiting 11 lines and a major (53.5%) one with C_2 symmetry exhibiting six lines.[17c]

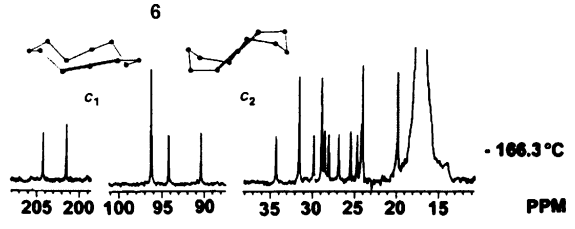

Figure 7. Low-temperature ^{13}C NMR spectrum (75.6 MHz in propane) of compound **6**. (Reprinted with permission from *J. Org. Chem.* **2003**, *68*, 3420–3424. Copyright 2003, American Chemical Society).

The barrier for the interconversion of the two topomers of C_1 symmetry was found to be equal to 8.4 kcal mol^{-1} and that for interconversion of the C_2-symmetric conformer into the C_1-symmetric topomers was found to be equal to 9.35 kcal mol^{-1}. Through theoretical calculations the structures of the conformers with C_1 and C_2 symmetries were identified as those displayed in Figure 7.

The single ^{13}C NMR line of cycloundecane (**7**) broadens on cooling and splits at –183 °C into two sets of lines corresponding to two distinguishable conformers with relative populations of 59 and 41%.[17b] The more populated conformer displays 11 sharp lines of equal intensity, the other two broad lines. On the basis of calculations (and by analogy with X-ray structures of similar compounds) the spectrum with 11 sharp lines was assigned to conformer **7a** (C_1 symmetry as in Figure 8), which does not appears to exchange any longer at this temperature.

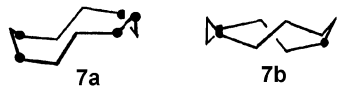

Figure 8. Computed (MM) low-energy conformations of cycloundecane (**7**). (Reprinted with permission from *J. Org. Chem.* **2006**, *71*, 6512–6515. Copyright 2006, American Chemical Society).

To the second conformer the structure **7b** (Figure 8) was assigned; this still exchanges the sites of its carbon atoms, thus exhibiting a time-averaged C_2 symmetry. Indeed, the computed barrier for this process (2.6 kcal mol^{-1}) is too low to be frozen on the NMR timescale at any attainable temperatures, whereas the **7a** to **7b** interconversion has a computed barrier (5.7 kcal mol^{-1}) high enough to account for the identification of two conformers at –183 °C.

4.2 Bond Rotations

The concept of axial chirality as a stereogenic source in a rotationally hindered compound was for many years relegated to the academic field. This situation was to change, however, with the discovery of many bioactive natural compounds containing stereogenic chiral axes and with the discovery of many catalysts useful for asymmetric synthesis. In particular, axially chiral biaryl systems have proven to be very efficient in the transfer of chirality.[69] The crucial aspect for the success of an axially chiral system is the conformational stability of the stereogenic axis under the reaction conditions. This implies that the rotational barrier must be greater than 25–26 kcal mol^{-1} or, more conveniently, greater than 30 kcal mol^{-1}. The most popular systems used for asymmetric synthesis contain the binaphthyl scaffold – such as BINAP or BINOL – or a highly hindered biphenyl system, but many others have been reported. The search for new atropoisomeric systems and the related conformational analysis is therefore an open research field. In this context, dynamic NMR, coupled with enantioselective HPLC and with DFT calculations, can help in the design of new scaffolds, through evaluation of the steric requirements needed

for the conformational stability of the chiral axis. A number of rotation processes involving carbon–carbon sp^2–sp^2, sp^2–sp^3, sp^3–sp^3 and sp–sp^2 bonds have been investigated in recent years.

4.2.1 sp^2–sp^2 Rotations

The most commonly investigated cases of sp^2–sp^2 restricted rotation relate to compounds containing two aryl groups bonded to an aromatic scaffold.[70] A selection of these cases is presented (Scheme 2).

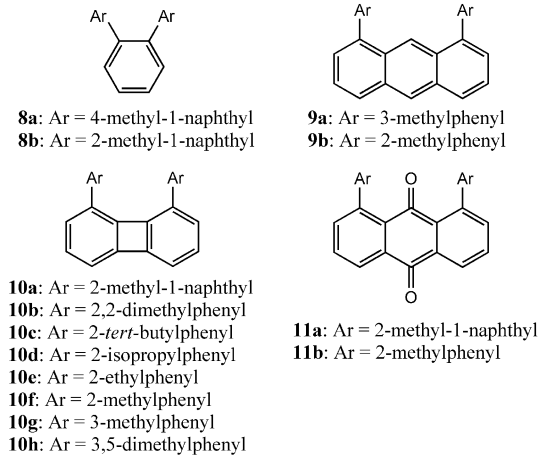

Scheme 2.

Compound **8a** exists as *syn* (*meso*) and *anti* (*racemic*) conformers (Figure 9).[71] These two forms were observed by NMR spectroscopy at ambient temperature and displayed a 1:1.6 intensity ratio under equilibrium conditions.

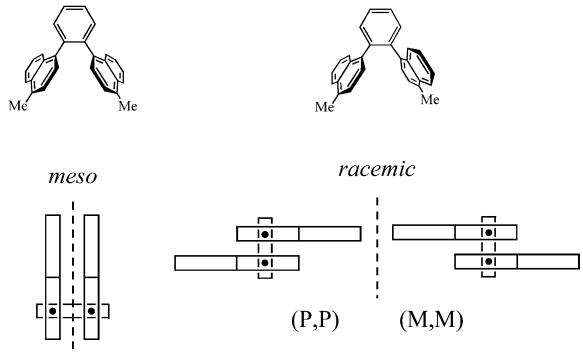

Figure 9. View of the two conformational diastereoisomers of hydrocarbon **8a**, with its naphthalene rings parallel (*syn*) or antiparallel (*anti*). (Reprinted with permission from *J. Org. Chem.* **2002**, *67*, 1663–1668. Copyright 2002, American Chemical Society).

By means of line shape simulation, variable-temperature NMR spectroscopy (Figure S-1 in the Supporting Information) provided the interconversion barrier for the major and the minor conformer ($\Delta G^{\neq}$ = 19.5 kcal mol^{-1}).

X-ray diffraction showed solely the *anti* form present in the crystal. This crystal was dissolved at low temperature (–55 °C) and the NMR spectrum was recorded without the temperature ever being raised (Figure S-2 in the Supporting Information) so that only the NMR spectrum of a single conformer was observed under these conditions. The spectrum observed in this experiment was found to correspond to that of the major conformer, which was therefore assigned the *anti* (i.e., racemic) structure.

Three peaks (due to the *meso* form and to the two *P*,*P* and *M*,*M* enantiomers) were observed at low temperature (–20 °C) by enantioselective HPLC. The use of an electronic circular dichroism (ECD) allowed the identification of the two chiral conformers, which display opposite phased peaks whereas the signal for the *meso* conformer is invisible (Figure 10). This experiment confirmed that the *anti* (racemic) conformer is the more populated form. Variable-temperature HPLC also yielded the barrier for the *anti* to *syn* interconversion. The value obtained in this way (19.4 kcal mol^{-1}) agrees well with the result of the NMR determination.

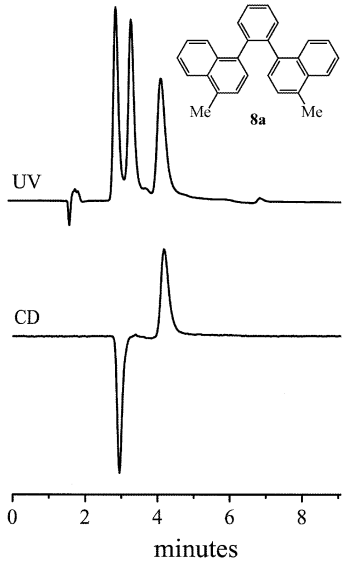

Figure 10. Chromatography of **8a** on enantiopure cellulose tris(3,5-dimethylphenyl carbamate) at –20 °C. Detection by UV (top) and ECD (bottom) at 230 nm. (Reprinted with permission from *J. Org. Chem.* **2002**, *67*, 1663–1668. Copyright 2002, American Chemical Society).

When the 4-methylnaphthyl groups of **8a** are replaced by the more hindered 2-methylnaphthyl groups (as in **8b**), the barrier increases up to the point of allowing a physical separation of the *meso* and *racemic* forms to be achieved. The latter, furthermore, could be separated into the *M*,*M* and *P*,*P* enantiomers by means of enantioselective HPLC (Figure S-3 in the Supporting Information).[72]

Anthracenes bearing two equivalent tolyl (*ortho* or *meta*) substituents at positions 1 and 8 (**9a** and **9b** in Scheme 2) generate *anti* and *syn* conformers that yield distinguishable NMR spectra.[73] In the case of the *meta* derivative **9a** the two forms were observed in a 63:37 ratio at –85 °C, with the *anti* form being more stable according to DFT calculations (Figure 11).

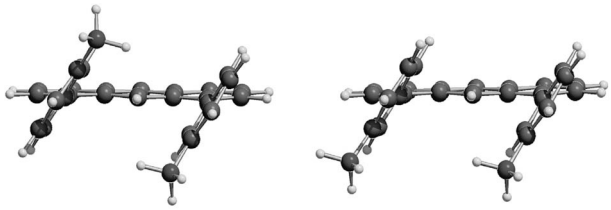

9a-anti (E = 0.0) **9a**-syn (E = 0.2)

Figure 11. Computed (DFT) structures [B3LYP/6-31G(d) level] of the *anti* and *syn* conformers of **9a**. The relative energies (*E*) are in kcal mol^{-1}. (Reprinted with permission from *J. Org. Chem*. **2007**, *72*, 5391–5394. Copyright 2007, American Chemical Society).

Contrary to a previous report,[74] the interconversion barrier ($\Delta G^{\neq}$) was found to be 11.2 kcal mol^{-1} and a very accurate line shape simulation allowed a negligible $\Delta S^{\neq}$ value of 1.1 ± 1 e.u to be ascertained. In the case of the *ortho* tolyl substituents (compound **9b**) the conformer populations are quite similar (53:47) but the interconversion barrier is much higher ($\Delta G^{\neq}$ = 21.2 kcal mol^{-1}), due to the increased steric effects.

Accordingly, the NMR spectra of the two conformers could be detected at ambient temperature. Again, line shape simulation indicated a negligible $\Delta S^{\neq}$ value of 0.75 ± 1 e.u., so the activation entropy in the conformational processes, in which there is no bond breaking, would be expected to be negligible (as reported in many other cases[75]); this should be taken into account even when an extremely accurate line shape simulation cannot be achieved for technical reasons.

Unambiguous assignment of the *anti* structure to the more populated conformation and of the *syn* structure to the less populated conformation could be achieved for compound **9b** by a novel and innovative NOE experiment[76] requiring the simultaneous irradiation of the ^{13}C satellites lines of the methyl groups. An enhancement was observed for the less intense methyl line but not for the more intense one (Figure 12). The former thus belongs to the *syn* conformer, in which the two enantiotopic methyl groups are sufficiently close to each other to display a NOE effect, whereas in the *anti* form they are too far apart to produce such an effect.

Biphenylenes bearing pairs of aryl groups lacking a C_2 symmetry axis in positions 1 and 8 (Scheme 2, compounds **10a**–**10h**)[77,78] give raise to *syn* (*meso*) and *anti* (racemic) forms. The barriers involved in the interconversion between the *syn* and *anti* conformers increase from 6.4 kcal mol^{-1} (**10g**) up to 34.5 kcal mol^{-1} (**10a**). In the latter compound the two forms are configurationally stable and could be separated. The *syn* isomer is the less populated (36% under equilibrium conditions) and the corresponding assignment was achieved by means of the NOE experiment[76] discussed above (see Figure S-4 in the Supporting Information).

The two enantiomers (*P*,*P* and *M*,*M*) of the *anti* isomer could be separated on an enantioselective HPLC column and the corresponding ECD spectra were recorded. TD-

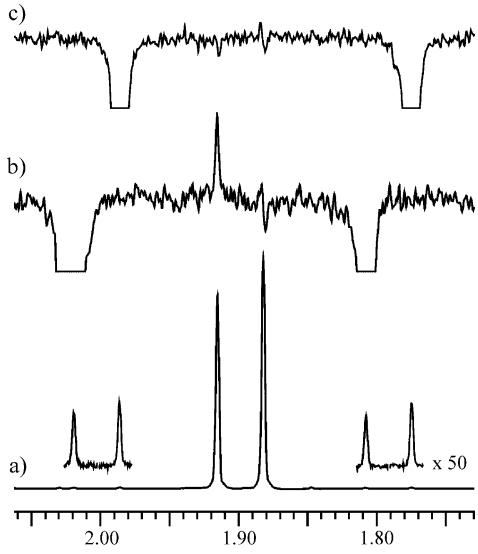

Figure 12. a) Methyl signals (^{1}H, 600 MHz) for **9b** in $CDCl_3$ at 0 °C, with the ^{13}C satellite signals in the inset. b) Spectrum obtained by simultaneous irradiation of the satellites of the downfield line (*syn* conformer). c) Spectrum obtained by simultaneous irradiation of the satellites of the upfield line (*anti* conformer). (Reprinted with permission from *J. Org. Chem*. **2007**, *72*, 5391–5394. Copyright 2007, American Chemical Society).

DFT computations[79] of the ECD spectrum of the *M*,*M* conformer agreed with that of the first eluted enantiomer (Figure 13), thus allowing the assignment of the absolute configuration.

When the two substituents are *meta*-xylene rings, the particular shape of the biphenylene scaffold allows the determination of a second stereodynamic process corresponding to the so-called "π-barrier",[80] which corresponds to a transition state in which the xylene ring is perpendicular to the biphenylene ring (Figure 14).

This barrier is usually too small to be detectable by dynamic NMR (about 2 kcal mol^{-1}),[81] but in the present case two features allow the process to be observed (the experimentally determined barrier is 6.3 kcal mol^{-1}, to be compared with the computed value of 4.6 kcal mol^{-1}): i) the ground state is more stabilised because of the presence of the central four-membered ring, which lowers the steric hindrance without altering the transition state energy, and ii) the barrier is doubled by the presence of two phenyl rings that are both involved in the transition state. DFT calculations reveal, in fact, that the two phenyl rings move in locked fashion, leading to a single transition state in which both the rings are perpendicular to biphenylene.

The *syn* and *anti* forms are also generated when the scaffold is the anthraquinone moiety. When the 1- and 8-substituents are *ortho*-toluenes (**11b**) they are stereolabile conformers,[82] whereas when the substituents are the more hindered 2-methyl-1-naphthyl groups (**11a**) the *syn* and *anti* isomers (red- and yellow-coloured, respectively, as in Figure S-5 in the Supporting Information) are sufficiently stable to be separated.[83]

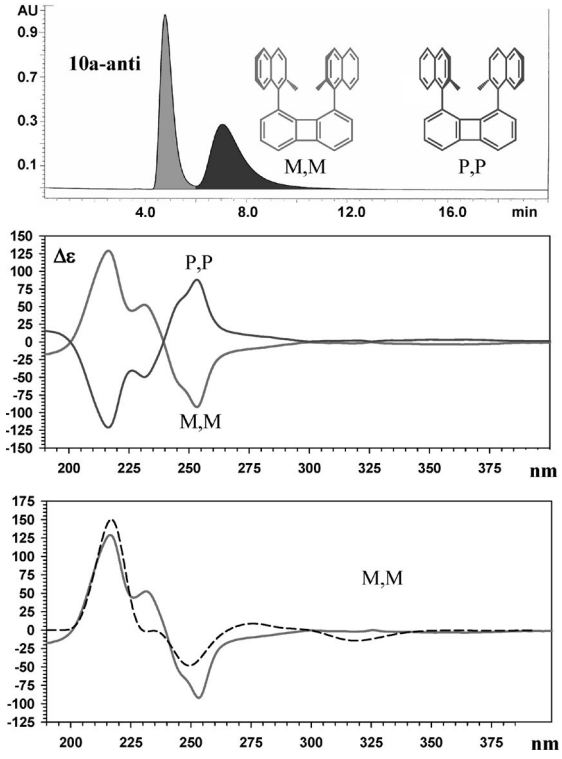

Figure 13. Top: enantioselective HPLC trace for the two enantiomers of **10a-*anti***. Middle: ECD spectra of the two enantiomers. Bottom: computed ECD spectrum (blue-shifted by 7 nm, dashed trace) for the *M*,*M* configuration, compared with the experimentally measured spectrum (full trace) of the first eluted enantiomer. (Adapted with permission from *J. Org. Chem.* **2008**, *73*, 2198–2205. Copyright 2008, American Chemical Society).

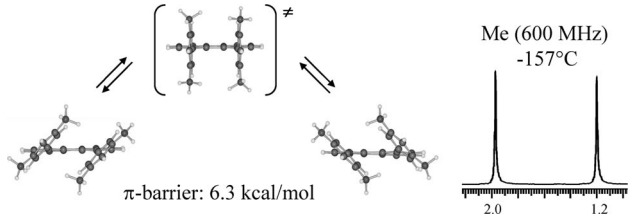

Figure 14. Bottom: computed (DFT) structures of the conformational enantiomers of **10h** (with dihedral angles of 43° between the planes of xylene and biphenylene). They exchange their inner and outer methyl groups on passing through the orthogonal transition state (top) through a 90° torsion. (Reproduced with permission from *J. Org. Chem.* **2007**, *72*, 10045–10050. Copyright 2007, American Chemical Society).

Their interconversion barrier has been determined as 35.4 kcal mol^{-1}, with the *anti* form more stable under equilibrium conditions (59:41 at +140 °C). Such an assignment was achieved by NOE performed by irradiation of the ^{13}C satellite lines of the enantiotopic methyl groups.[76] X-ray diffraction confirmed the structural assignment in the case of the *syn* isomer (Figure 15). The *anti* isomer is racemic and the two *P*,*P* and *M*,*M* isomers were separated by enantioselective HPLC. The ECD spectrum of the first eluted enantiomer was satisfactorily reproduced by TD-DFT computations[79] for the *M*,*M* enantiomer, thus allowing the assignment of the absolute configuration (Figure S-6 in the Supporting Information).

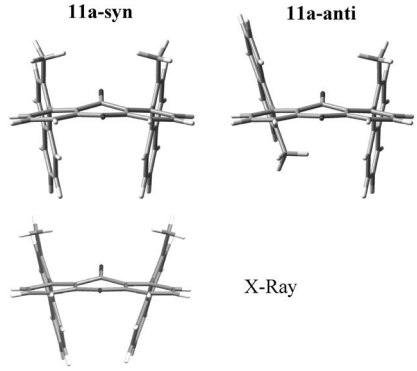

Figure 15. Top: computed (DFT) ground states of **11a-*syn*** and **11a-*anti***. Underneath is the X-ray structure determined for the *syn* isomer. (Reproduced with permission from *J. Org. Chem.* **2009**, *74*, 1345–1348. Copyright 2009, American Chemical Society).

4.2.2 sp^3–sp^3 Rotations

Studies of conformations of small molecules each based on a quaternary carbon centre bearing four equal alkyl substituents (**12**–**19**) have recently been reported (Scheme 3).

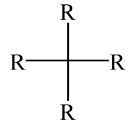

12: R = *i*Pr
13: R = cyclopropyl
14: R = Et
15: R = *n*Pr
16: R = CH_2Cl
17: R = CH_2Br
18: R = CH_2Ph
19: R = CH_2-cyclopropyl

Scheme 3.

Tetraisopropylmethane (**12**) can adopt 81 (i.e., 3^4) possible conformations, which fall into the six types T1–T6 shown in Figure 16. According to MM3 calculations, the most stable, called T1, is threefold degenerate and the second-most stable (T3) is sixfold degenerate.[84]

The low-temperature (–115 °C) ^{1}H NMR spectrum of **12** shows two distinguishable CH multiplets with a 93:7 intensity ratio. The $\Delta G^{\neq}$ value for the interconversion is 9.7 kcal mol^{-1}, as derived from the rate constants (k) used for the line shape simulation (Figure 17).

The corresponding methyl signal of the major conformer is a doublet (due to the coupling with CH) whereas the minor methyl signal comprises two overlapping doublets (Figure S-7 in the Supporting Information). These observations are consistent with the symmetries of the two most stable conformers predicted by computations. The major one (T1) in fact has D_{2d} symmetry and the minor one (T3) S_4 symmetry. The former has eight equivalent methyl groups whereas the latter is expected to have distinct geminal methyl groups, thus yielding two doublet signals, each corresponding to four equivalent methyl groups.

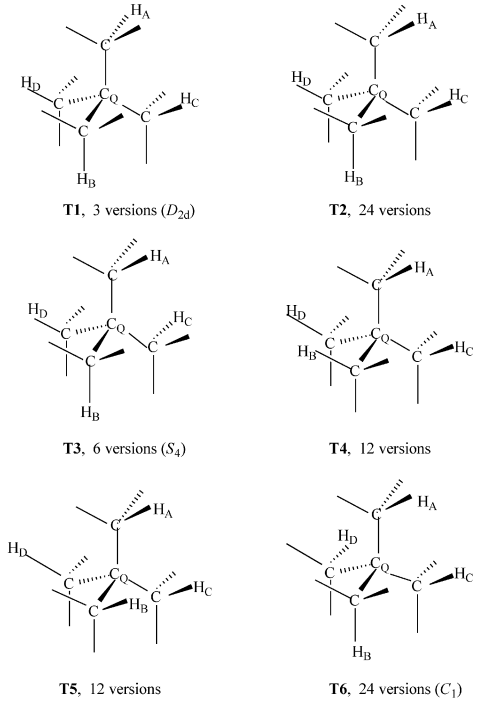

Figure 16. Schematic representation of the six conformational types of compound **12**. (Adapted with permission from *J. Am. Chem. Soc.* **2002**, *124*, 6706–6713. Copyright 2002, American Chemical Society).

The analogous tetracyclopropylmethane (**13**) also has six possible conformers but here the most stable is computed to be T3 (S_4 symmetry, sixfold degenerate) and the second-most stable is T6 (C_1 symmetry, 24-fold degenerate). In this compound the internal motions are much faster than in the previous one and only at –180 °C does the ^{13}C NMR spectrum display a 1:1 splitting of the methylene signal (Figure 18).

This feature confirms that, as anticipated by computations, the major conformer is indeed T3, in which there are two sets of CH_2 groups, each comprising four equivalent methylenes. Under such extreme conditions the NMR lines are quite broad, so even if a second conformer with a much smaller population is present, the corresponding NMR signals cannot be experimentally detected. The interconversion barrier computed for the internal motion that renders all the CH_2 groups equivalent is 3.6 kcal mol^{-1}, a value in satisfactory agreement with the experimentally measured 4.5 kcal mol^{-1}.

In the case of tetraethylmethane[85] (**14**), MM computations indicate that of the six possible conformational types, the two most stable are T1 (threefold degenerate) and T3 (sixfold degenerate). At –155 °C the ^{13}C NMR spectrum of **14** shows two signals corresponding to methylene carbons and due to the two conformers (T1 and T3) predicted by computations, which interconvert with an experimentally determined barrier of 6.6 kcal mol^{-1}. The value computed by Adler et al.[86] is also 6.6 kcal mol^{-1}. The ^1H NMR spectrum of **14** at –157 °C shows a sharp methylene quartet (owing to the coupling with CH_3) for the major signal (compat-

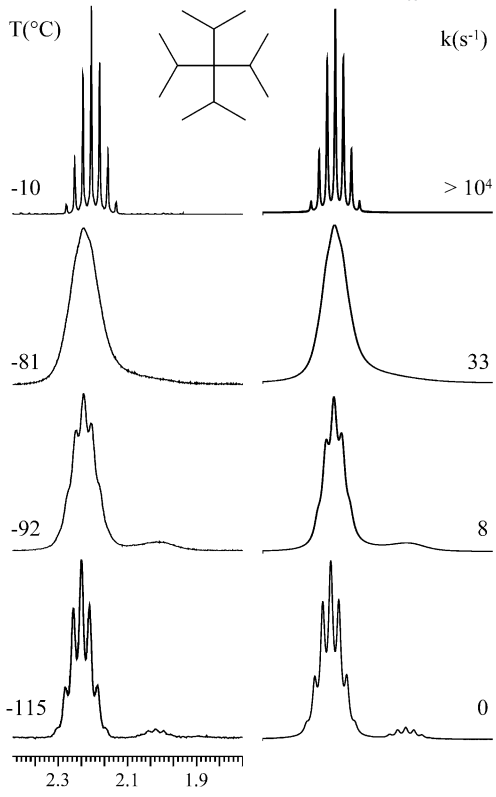

Figure 17. Temperature dependence of the experimentally measured (left) and computer-simulated (right) CH signal (^1H at 400 MHz in CD_2Cl_2) of compound **12**. (Reproduced with permission from *J. Am. Chem. Soc.* **2002**, *124*, 6706–6713. Copyright 2002, American Chemical Society).

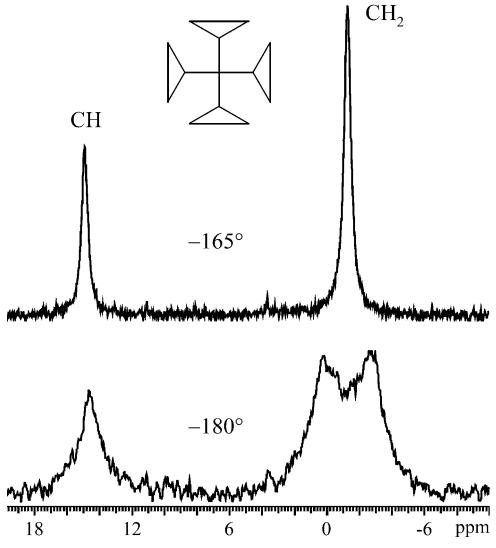

Figure 18. ^{13}C NMR signals (125.7 MHz) corresponding to the CH and CH_2 carbons of tetracyclopropylmethane (**13**) in CHF_2Cl/$CHFCl_2$ at two different temperatures. Top: at –165 °C the methylene carbons still display a single line. Bottom: at –180 °C, however, this is split into a pair of equally intense lines. (Adapted with permission from *J. Am. Chem. Soc.* **2002**, *124*, 6706–6713. Copyright 2002, American Chemical Society).

ible with the D_{2d} symmetry of conformer T1) and a very broad CH_2 line for the minor conformer. This feature supports the assignment of the latter signal to the T3 conformer, because its corresponding S_4 symmetry entails diastereotopic geminal hydrogen atoms for CH_2, which should provide the AB portion of an ABX_3 system. It is worth noting that an electron diffraction study of **14** in the gaseous phase also indicated the presence of two conformers, T1 being more stable than T3.[87]

An even clearer indication of the presence of both T1 and T3 conformers in compounds of this type is offered by the ^1H NMR spectrum of the analogous $C(CH_2Cl)_4$ (**16**). At –158 °C, in fact, the major CH_2 signal is a single line, as would be expected for the D_{2d} symmetry of T1, whereas the minor signal displays the four lines of an AB-type spectrum (Figure 19) because the geminal CH_2 hydrogen atoms are diastereotopic (and thus coupled to each other with J = –11 Hz), corresponding to the previously mentioned S_4 symmetry of T3.

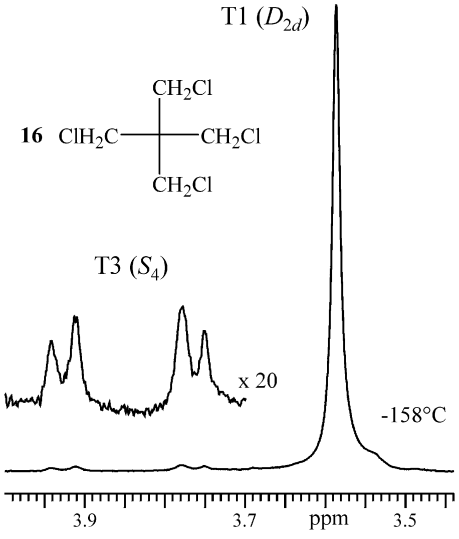

Figure 19. ^1H NMR spectrum (400 MHz) of tetra(chloromethyl)-methane (**16**) in $CHF_2Cl/CHFCl_2$ at –158 °C, showing signals for type T1 (D_{2d} symmetry) and type T3 (S_4 symmetry) conformations: a singlet and an AB multiplet, respectively (the latter appears in the inset with a 20-fold amplification). (Adapted with permission from *J. Org. Chem.* **2002**, *67*, 6387–6394. Copyright 2002, American Chemical Society).

In the case of compound **19** the ^1H NMR spectrum at –161 °C shows that the exocyclic methylene hydrogen atoms are diastereotopic (Figure S-8 in the Supporting Information), due to the freezing of the Cq–CH_2 bond rotation. This also indicates that the molecule has adopted S_4 symmetry corresponding to conformer T3. Unlike in the cases of **14**–**17**, only a single conformer appears to be populated, a result consistent with ab initio [RHF 6-31G(d) level] computations predicting that the energy difference with respect to the second most stable conformer T1 is as large as 1.34 kcal mol^{-1}. The structure derived from the NMR spectroscopic data and from calculations very closely matches that determined by X-ray diffraction in the solid state[88] (see Figure S-9 in the Supporting Information).

4.2.3 sp^3–sp^2 Rotations

Variable-temperature NMR spectroscopy was capable of detecting restricted rotation about the sp^2–sp^3 bonds in hindered aryl carbinols[89] and of measuring the corresponding barriers. Pairs of stereolabile atropisomers with different populations were observed with aryl ring lacking twofold symmetry axes. When highly hindered compounds were examined, the atropisomers were configurationally stable and could be physically separated.

Hindered carbinols of the general formula shown in Scheme 4 give rise, in the cases of compounds **20**–**22**, to *sc* (synclinal) and *ap* (antiperiplanar)[90] conformational atropisomers,[91] as illustrated in Figure 20.

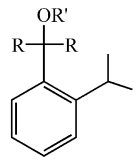

20: R = Me, R' = H
21: R = Et, R' = H
22: R = *i*Pr, R' = H
23: R = *t*Bu, R' = H
24: R = Me, R' = Me
25: R = Et, R' = Me
26: R = *i*Pr, R' = Me
27: R = *t*Bu, R' = Me

Scheme 4.

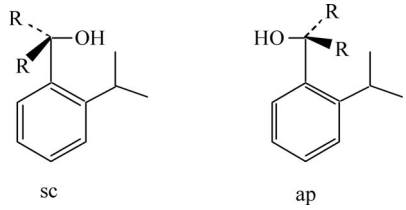

Figure 20. Schematic representation of *sc* and *ap* atropisomers of compounds **20**–**23** (Reprinted with permission from *J. Org. Chem.* **2005**, *70*, 5098–5102. Copyright 2005, American Chemical Society).

Their relative proportions can be determined by low-temperature NMR spectroscopy, which displays separate signals corresponding to the two conformers. Computer simulation of the line shape at different temperatures also allows one to obtain the interconversion rates: the corresponding free energies of activation involved in these processes were found to cover the 7.6–13.5 kcal mol^{-1} range. One such example, for derivative **20** (R = Me), is shown in Figure S-10 in the Supporting Information.

Structural assignment of the two atropisomers can be proposed on the basis of the energies derived by DFT calculations, but experimental determination can also be achieved by means of NOE experiments carried out at a temperature sufficiently low to yield distinguishable spectra for the two conformers.

In the case of compound **22** (R = *i*Pr), for instance, the NOE spectra (Figure 21) obtained by irradiation of the CH signals of the *ortho* isopropyl groups at –80 °C are shown. When the major CH signal is irradiated (trace c) enhancement of the OH signal is observed, whereas when the minor signal is irradiated (trace b) the effect occurs on the CH signal corresponding to the two equivalent (enantiotopic) isopropyl groups bonded to the COH moiety. This unambiguously shows that the *sc* conformational atropisomer is the more stable form (82%), a result consistent with the

computational prediction (this makes the results of these calculations quite reliable, so that they can accordingly be confidently used for assignments of compounds of this type). It is worth outlining that the X-ray structure of **20** also supports the computational conclusions, by showing that the more stable *sc* structure is the one found in the crystal (see Figure S-11 in the Supporting Information).

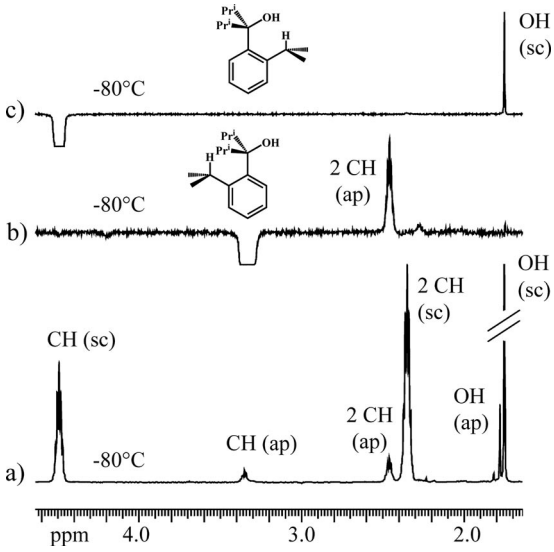

Figure 21. NOE experiments (600 MHz at –80 °C in CD_2Cl_2) carried out by excitation of the CH multiplet of the *ortho*-isopropyl group in the minor and major atropisomers of compound **22** (traces b and c, respectively). The control spectrum in the region 1.6–4.6 ppm (trace a) is also shown. (Reprinted with permission from *J. Org. Chem.* **2005**, *70*, 5098–5102. Copyright 2005, American Chemical Society).

A second conformational process in the *sc*-atropisomer of **22** becomes NMR-visible when this compound is further cooled to about –150 °C: the CH signal of the two equivalent isopropyl groups bonded to the COH moiety splits into a pair of anisochronous signals as this atropisomer adopts an asymmetric, and thus chiral, conformation in which the isopropyl groups are diastereotopic. The barrier measured for this process (6.4 kcal mol^{-1}) is reasonably matched by DFT computations.

The NMR spectrum of **23** (R = *t*Bu), on the other hand, indicated that the reaction produces only one of the two possible atropisomers, with NOE experiments identifying its structure as that with the *ap* disposition. On warming, however, this atropisomer was completely interconverted into its *sc* companion (also identified by NOE) thus showing the latter to be thermodynamically more stable, as predicted by calculations (the presence of the *ap* atropisomer is therefore the result of a kinetically controlled reaction). The barrier measured for the interconversion of these atropisomers is high enough (29.3 kcal mol^{-1}) to identify these forms as stable diastereoisomers, rather than stereolabile conformers as in the case of compounds **20**–**22**.

When the hydrogen is substituted by a methyl group,[92] the resulting benzyl ethers **24**–**27** (Scheme 4), are predicted (DFT computations) to adopt mainly a synclinal (or synperiplanar) conformation in which the OMe group points towards the *ortho* alkyl substituent. This prediction is confirmed by NOE experiments in the case of compound **24** and by X-ray diffraction in the case of **27**.

The low-temperature (–151 °C) ^{13}C NMR spectrum of **24** did not show the presence of two conformations, but the presence of a single asymmetric (and thus chiral) conformer. In fact, two anisochronous signals are observed for the two methyl groups bonded to the COMe moiety, owing to the freezing of the rotation about the Ar–COMe bond. The chirality of this conformation is corroborated by the *ortho* isopropyl group displaying two anisochronous Me signals, despite the fast Ar–isopropyl rotation (a situation that is expected to occur whenever the isopropyl group acts as a chirality probe in an asymmetric structure).[93] The barrier involved in this process was measured as 6.6 kcal mol^{-1}. In the case of compound **26** in addition to the major synclinal conformer two slightly different antiperiplanar minor conformers (with 4% and 9% proportions; see Figure S-12 in the Supporting Information) were observed in the low-temperature NMR spectra, as predicted by computations.

Another example of sp^3–sp^2 restricted rotation is offered by compounds **28**–**32** (Scheme 5). The structure of compound **28** was predicted by DFT computations and confirmed by X-ray diffraction (Figure S-13 in the Supporting Information). The low-temperature NMR spectra allowed the determination of the rotation barrier of the 4-methoxyphenyl group (10.2 kcal mol^{-1}) and also that of the 3-methylphenyl substituent (10.8 kcal mol^{-1}), the latter corresponding to an enantiomerisation process between two stereolabile atropisomers (enantiomers).[94]

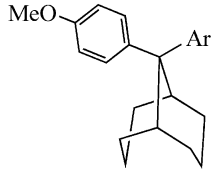

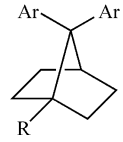

28: Ar = 3-methylphenyl
29: Ar = 2-methylphenyl
30: Ar = 1-naphthyl

31: Ar = phenyl, R = Me
32: Ar = 4-methoxyphenyl, R = phenyl

Scheme 5.

If a larger substituent such as, for instance, the 1-naphthyl moiety (compound **30**) replaces the 3-methylphenyl group, the rotation barrier of the 4-methoxyphenyl group is reduced to 5.15 kcal mol^{-1} whereas that of the 1-naphthyl becomes so high (≥25 kcal mol^{-1}) as to make the corresponding atropisomers (enantiomers) configurationally stable. They could thus be separated on an enantioselective HPLC column and the corresponding ECD spectra recorded (Figure 22).

It was suggested, on the basis of the exciton chirality rules of Nakanishi et al.,[95] that the *M* absolute configuration should be assigned to the first eluted enantiomer. Here we also show that the computed (TD-DFT) ECD spectrum of the *M* enantiomer does indeed correspond to the experimentally measured spectrum of the first eluted enantiomer (Figure S-14 in the Supporting Information).

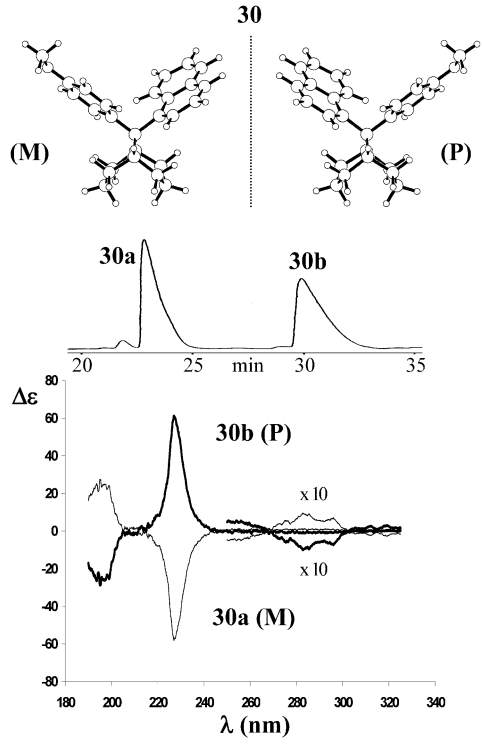

Figure 22. Top: HPLC trace of the atropisomers of **30**. Bottom: ECD spectra of the atropisomers of **30**. The absolute configuration *M* was assigned to the first eluted atropisomer **30a**. (Adapted with permission from *J. Org. Chem.* **2003**, *68*, 1815–1820. Copyright 2003, American Chemical Society).

Restricted rotations of an analogous type were measured by ^{13}C NMR in the norbornane derivatives **31** and **32**, in which the barriers are 7.9 and 6.0 kcal mol^{-1}, respectively.[96] The potential energy surface for compound **31** was calculated by MM methods, showing that the two phenyls rotate independently of each other (Figure S-15 in the Supporting Information). In the case of **32** the computed conformation was found to be in agreement with the experimentally determined X-ray structure.

4.2.4 sp–sp² Rotations

A quite unusual example of restricted sp–sp^2 rotation is offered by the crowded derivatives **33**–**36** (Scheme 6).[97]

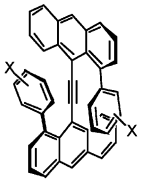

33, X = 4-Me
34, X = 4-*i*Pr
35, X = 3-*i*Pr
36, X = 3,5-*i*Pr$_2$

Scheme 6.

The variable-temperature ^1H NMR spectrum of compound **36** indicates the existence of two distinct dynamic processes. Over the range from –74 to +63 °C the four methyl signals of the isopropyl groups of **36** broaden and coalesce, eventually displaying only two signals. In addition, the two CH isopropyl signals broaden and coalesce into a single signal over the same temperature range. In the range from +63° to +140 °C the two isopropyl methyl signals broaden further and coalesce into a single signal, but this process does not affect the CH signal (Figure S-16 in the Supporting Information, top). Line shape analysis demonstrated that the two barriers ($\Delta G^{\neq}$) involved in these dynamic processes are 11.9 and 18.0 kcal mol^{-1}.

As shown in Figure S-16 in the Supporting Information (bottom), one of the two pathways corresponds to the rotation of the phenyl ring (PR) with respect to the anthracene ring (lower barrier); that is, a topomerisation involving site exchange of two isopropyl groups in each phenyl moiety. The other pathway corresponds to the rotation about the acetylene axis (AR) and leads to enantiomerisation of two staggered conformers with a stereogenic axis (higher barrier); that is, site exchange of diastereotopic methyl groups in each isopropyl substituent.

4.3 Nitrogen Inversion

Detailed reviews of inversion/rotation processes were published in 1992.[98–100] More recent results, involving compounds **37**–**42** (Scheme 7), are reported here.

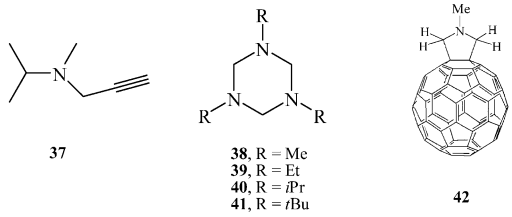

37

38, R = Me
39, R = Et
40, R = *i*Pr
41, R = *t*Bu

42

Scheme 7.

The ^{13}C line corresponding to the isopropylmethyl group of *N*-isopropyl-*N*-methylpropargylamine (**37**) splits at about –120 °C (Figure S-17 in the Supporting Information) into a pair of lines, indicating that the N-inversion process is slow on the NMR timescale at this temperature.[101] Under these conditions the nitrogen atom is chiral and, accordingly, makes the two isopropyl methyl groups diastereotopic.[93] The enantiomerisation barrier ($\Delta G^{\neq}$) corresponding to the nitrogen inversion/rotation process was measured as 7.7 kcal mol^{-1}. Support for this interpretation is provided by the ^1H NMR spectrum of the CH_2 hydrogen atoms that yield, at the same temperature, an AB-type spectrum (geminal J = –18 Hz) because these hydrogen atoms are also made diastereotopic by the pyramidal nature of the nitrogen. Calculations indicate that the AA form[102] shown in Figure 23 corresponds to the dominant conformer.

The saturated 1,3,5-trialkyl-1,3,5-triazacyclohexanes **38**–**41** [alkyl = Me (**TMTAC**), Et (**TETAC**), *i*Pr (**TPTAC**) and *t*Bu (**TBTAC**)] generally show a strong preference for the chair conformation over the twist form.[103] ^1H NMR spectra in the range from +57 to –83 °C show a decoalescence of the ring methylene protons due to slowing of the chair-

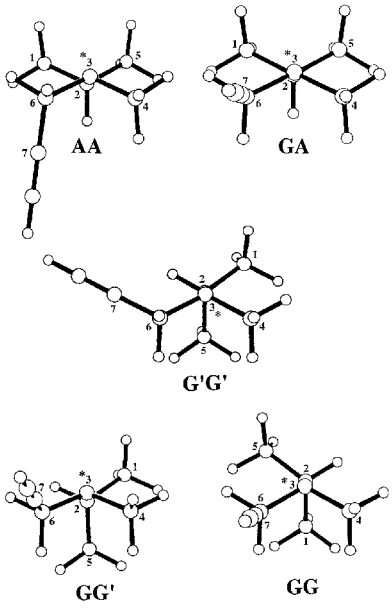

Figure 23. **AA**, **GA**, **G′G′**, **GG′** and **GG** conformations of **37**. Nitrogen is indicated by an asterisk (*S* configuration). (Adapted with permission from *J. Org. Chem*. **2001**, *66*, 903–909. Copyright 2001, American Chemical Society).

to-chair interconversion. The free energies of activation cover the range from 12.8 to 10.3 kcal mol^{-1} and decrease with the steric hindrance of the alkyl groups.

With a further decrease in the temperature, both the ^{1}H and ^{13}C NMR spectra show a second decoalscence due to nitrogen inversion, which suggests a strong preference for the conformation with an axial alkyl group (three equivalent: *aee*, *eae*, *eea*), whereas the expected triequatorial form (*eee*) can be observed only in a small amount. The free energies of activation for the interconversion between monoaxial conformations through sequential nitrogen inversion cover the 7.3–5.7 kcal mol^{-1} range and decrease with the steric hindrance of the alkyl substituents.

In compound **41**, the decoalescence of the *t*Bu into multiple signals at –168 °C is consistent both with nitrogen inversion and with *t*Bu rotation being slowed. However, simulations of the experimental traces are successful only if rotation is considered to occur in concert with nitrogen inversion. This implies that the isolated rotation barriers for equatorial and axial *t*Bu groups are equal to or higher than those for nitrogen inversion.[104]

In a solvent that does not make hydrogen bonds (CF_2Cl_2) the ^{1}H NMR spectrum of **38** at –147 °C shows only a monoaxial form (Figure 24), whereas in a solvent that can make hydrogen bonds (CHF_2Cl) the spectrum of **38** at –146 °C still shows a dominant monoaxial conformation but also 1% of the *eee* conformer. The *eaa* conformation is presumed to be too unstable to be populated at the equilibrium, and no diaxial conformations are detected in either solvent. Nevertheless, calculations predict that the energy required for the *eea* to *eaa* inversion is 0.6 kcal mol^{-1} lower than that for the *eea* to *eee* nitrogen inversion. For **38** and **39**, this corresponds to a preferred equilibrium between the monoaxial forms via the *eaa* conformation rather than via the *eee* conformation (Figure 25).

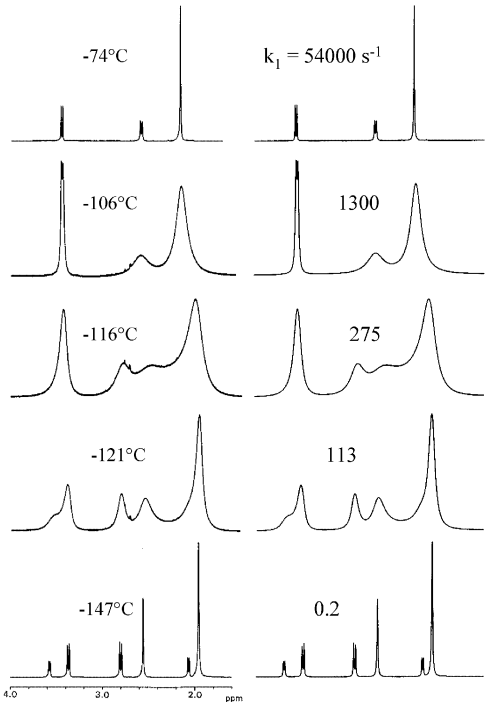

Figure 24. Left: experimentally measured ^{1}H DNMR spectra (500.16 MHz) of **38** (3% v/v in CF_2Cl_2). Right: theoretical simulations. The rate constant (k_1) is associated with conversion of one monoaxial conformation into one other monoaxial conformer. (Adapted with permission from *J. Am. Chem. Soc.* **2000**, *122*, 308–323. Copyright 2000, American Chemical Society).

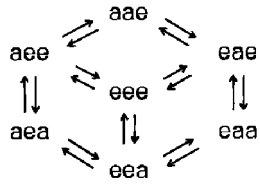

Figure 25. Conformational exchange between various stable and unstable equilibrium conformations of a chair conformer of **38** (**e** = equatorial methyl; **a** = axial methyl) by nitrogen inversion. (Reprinted with permission from *J. Am. Chem. Soc.* **2000**, *122*, 308–323. Copyright 2000, American Chemical Society).

The ^{1}H NMR spectrum of **41** at –168 °C in a non-hydrogen-bonding solvent shows only a monoaxial conformation, whereas a significant reversal of conformation preference, for the *eee* form, is observed in a hydrogen-bonding solvent at –161 °C. This enhanced preference for the *eee* conformation in **41** is attributable to several factors, such as the increased steric repulsion experienced by the *t*Bu methyl groups in the axial group, which have to reside over the ring, and the mitigation of the anomeric effect in large part due to hydrogen bonding. Mitigation of the anomeric effect in **38** and **39**, due to hydrogen bonding, results in the presence of about 1% of the *eee* conformation.

Ab initio and modified MMX (MMXTAC) computations are consistent with the experimental data and show that for the *eee* conformations of all the trialkyl triazacyclohexanes the C–N–C(axial) bond angles are affected by the hindrance due to the alkyl groups and that the pyramidality at nitrogen progressively decreases. This is consistent with the progressively decreasing barriers to nitrogen inversion and to chair-to-chair interconversion.

Calculations for the intermediate *eaa* conformers of **41** suggest that they are too high in energy for interconversion of the monoaxial forms. The only reasonable intermediate turns out to be the *eee* conformation. It thus appears that two monoaxial forms of **41** interconvert via *eee* as the sole intermediate, whereas in the case of **38** this is unlikely.

The pyrrolidino-fullerene **42** displays a N-inversion process in that the ^{1}H single line corresponding to the four hydrogen atoms of the two methylene groups splits into two signals with a 1:1 intensity at –90 °C, whereas the NMe line does not (Figure S-18 in the Supporting Information).[105] As a result of the restricted nitrogen inversion the four methylene hydrogen atoms become diastereotopic, two assuming a *syn* and two an *anti* position with respect to the NMe moiety. Line shape simulation provided a free energy of activation ($\Delta G^{\neq}$) of 8.65 kcal mol^{-1} ($\Delta H^{\neq}$ = 8.5 kcal mol^{-1} and $\Delta S^{\neq}$ = –0.8 e.u.), values in keeping with the expectations for a N-inversion barrier.

4.4 Miscellanea

An example of Ar–Ar rotation in combination with an unusual inversion process has been reported in the case of the bis-corannulene **44** (Scheme 8).[106] Corannulene (**43**) is a bowl-shaped molecule that interconverts rapidly at ambient temperature. The barrier for such a process (10.2 kcal mol^{-1}) was measured by making use of a substituent that acted as a diastereotopicity probe,[107] displaying a single NMR line at ambient temperature but a pair of equally intense lines at –90 °C. This established that the corannulene moiety is not planar and that at low temperatures the bowl did not interconvert any longer on the NMR timescale.

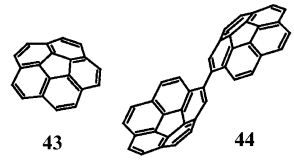

Scheme 8.

The $C_{40}H_{18}$ bis-corannulene compound **44**, consisting of two corannulene moieties joined together, displays stereodynamic processes involving the Ar–Ar bond rotation, in addition to the corannulene bowl inversion (Figure 26).

The ^{1}H NMR spectrum at ambient temperature (a singlet and eight doublets) resolves at –90 °C to reveal the presence of three sets of spectra (**a**, **b**, **c** as in Figure S-19 in the Supporting Information) corresponding to three diastereomeric conformers in 69:28:3 ratio. The enantiomers arising from Ar–Ar rotation are labelled *S* and *R* and those due to the bowl inversion *M* and *P*. On the basis of DFT calculations the observed conformers were assigned the configurations *S.PP*/*R.MM* (**a**), *S.MM*/*R.PP* (**b**) and *S.PM*/*R.MP* (**c**).

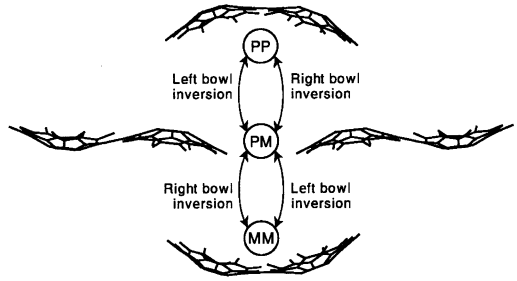

Figure 26. Combinations of bowl-shaped corannulenyl moieties and transitions between them, with the dihedral angle between the bowls fixed at 180° (note that at this dihedral angle the *PM* and *MP* combinations are identical). (Reprinted with permission from *J. Org. Chem*, **2008**, *73*, 6073–6078. Copyright 2008, American Chemical Society).

This assignment was further supported by symmetry considerations, because the spectra of **a** and **b** are compatible with C_2 symmetry whereas that of **c** corresponds to a structure without any element of symmetry, as predicted by computations. X-ray diffraction of **44** shows that the most stable form is indeed *S.PP*/*R.MM*, consistently with the NMR and computation assignment. The interconversion pathway between the conformers is quite complex and has been theoretically analysed (Figure 27). It appears that the most favourable enantiomerisation pathway passes through one of the two achiral transition states.

An example of dynamic motion involving distortion of a conjugated system from planarity has recently been reported.[108] 1,4,5,6,9,12-Hexamethyltriphenylene (compound **45**, Scheme 9) might, in principle, adopt either a C_2 or a D_3 conformation.

Whereas in the D_3 conformation the six methyl groups and the six aromatic hydrogen atoms are all equivalent, in the C_2 conformation there is a group of four equivalent methyl groups and four equivalent aromatic hydrogen atoms that are distinguishable (diastereotopic) from the other two, thus leading to a chiral situation. Computations predict C_2 to be far more stable than D_3, but the NMR spectrum at ambient temperature displays a single line for the six methyl groups and also one for the six aromatics. On cooling to –80 °C, however, both the methyl and the aromatic signal split into a pair of lines with a 4:2 intensity ratio, as predicted for a C_2 conformer (Figure S-20 in the Supporting Information). It is thus established that C_2 is the preferred conformation and that rapid inversion (enantiomerisation), occurring with a $\Delta G^{\neq}$ value of 10.6 kcal mol^{-1}, is responsible for the apparent D_3 symmetry observed at ambient temperature. Computations also suggest that the enantiomerisation pathway takes place through flipping mechanisms proceeding through low-en-

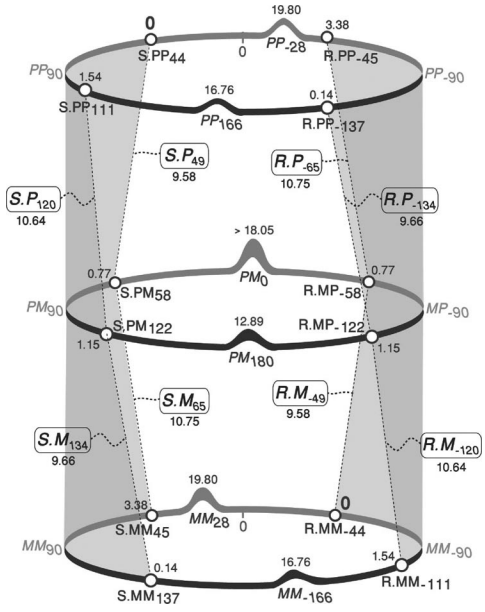

Figure 27. Stereodynamics map for bicorannulenyl (**44**). Stable conformations are represented by circles. The exact names (which include the DFT-calculated dihedral angles) are given for all 12 conformations and 16 transition states. The numbers represent calculated energies in kcal mol^{-1}, relative to the lowest-energy conformation (*S.PP*$_{44}$/*R.MM*$_{-44}$,) at 298.15 K. (Reprinted with permission from *J. Org. Chem*, **2008**, *73*, 6073–6078. Copyright 2008, American Chemical Society).

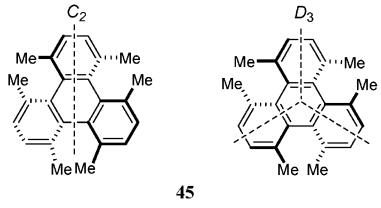

Scheme 9.

ergy C_s transition states (Figure 28). X-ray diffraction confirms that this molecule also adopts C_2 symmetry in the crystalline state.

An example of rotation involving a heteroatom such as phosphorus is reported for compounds **46** and **47**,[109] as in Scheme 10.

9-Diisopropylphosphanyl anthracene (**46**) adopts a staggered conformation, which thus gives rise to distinguishable ^{1}H NMR signals for the hydrogen atoms at the 1- and 8-positions of the anthracene moiety (Figure 29).

When the temperature was raised above –25 °C (see Figure S-21 in the Supporting Information) these signals coalesced, yielding a barrier for the Ar–P rotation of 13.3 kcal mol^{-1}.

Accordingly, when two P(*i*Pr)$_2$ groups are present at the 9- and 10-positions of anthracene (compound **47**) two conformers (labelled *cisoid* and *transoid*) are observed: they yield distinguishable NMR spectra at –50 °C (Figure S-22 in the Supporting Information). The spectral assignment was achieved on the basis of symmetry considerations: in

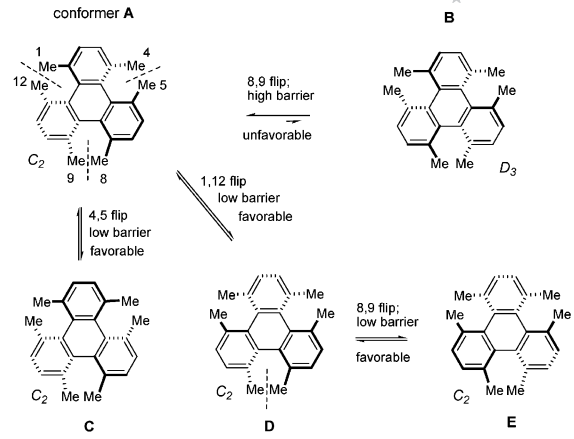

Figure 28. Wedge drawings of **45**, illustrating the rapid conformational interconversions that produce averaged ^{1}H NMR signals. Computations indicate that the mechanism proceeds chiefly through successive low-barrier C_2–C_2 interchanges. (Reprinted with permission from *J. Am. Chem. Soc.* **2007**, *129*, 13193–13200. Copyright 2007, American Chemical Society).

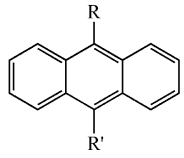

46, R = P(*i*Pr)$_2$, R' = H
47, R = R' = P(*i*Pr)$_2$

Scheme 10.

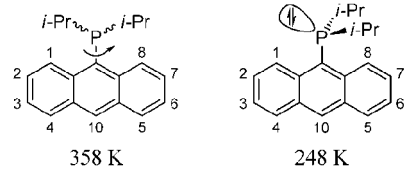

Figure 29. Temperature-dependent conformations of **46** (Reprinted with permission from *J. Org. Chem.* **2008**, *73*, 5242–5247. Copyright 2008, American Chemical Society).

the *cisoid* form the signals of the hydrogen atoms at the 1- and 4-positions are equivalent, as are the pair at the 5- and 8-positions, whereas in the *transoid* form the 1,5 and 4,8 pairs are equivalent. The *transoid* to *cisoid* ratio was measured as 57:43, and X-ray diffraction indicates that the more stable *transoid* structure is the only form present in the crystalline state.

Examples of molecules exhibiting three internal motions (phenyl rotation, *t*Bu rotation and N-inversion) have been reported for amino alcohols.[110] Because of the presence of two chiral carbon atoms, the Me$_2$NCH$_2$CHMe(OH)Ph*t*Bu system exists as four stereoisomers: a pair of diastereoisomers, each consisting of two enantiomers. The racemic compound **48** was identified as having the *R*,*R* and *S*,*S* configurations and the racemic **49** the *R*,*S* and *S*,*R* configurations (Figure 30).

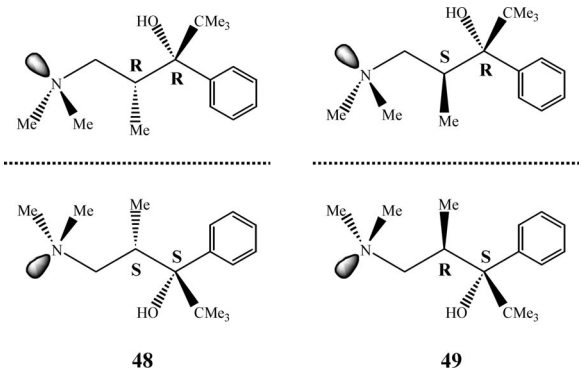

48 **49**

Figure 30. Schematic representation of the four stereoisomers of **48** and **49** (Reprinted with permission from *J. Org. Chem*. **2002**, *67*, 2659–2664. Copyright 2002, American Chemical Society).

Both **48** and **49** display restricted C–Ph and C–*t*Bu rotation; in addition they also display a N-inversion dynamic process. The ^{13}C signal corresponding to the Me_2N component, for instance, is split into two equally intense lines at –92 °C (Figure 31).

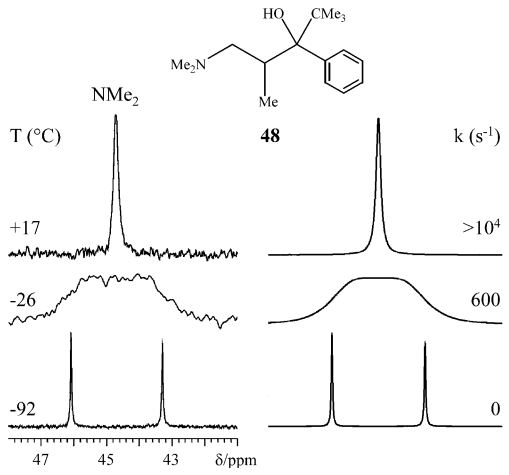

Figure 31. Left: experimentally measured ^{13}C NMR (100.6 MHz in CD_2Cl_2) signals corresponding to the *N*-methyl group of **48** as a function of temperature. Right: computer simulation with the reported rate constants. (Reprinted with permission from *J. Org. Chem*. **2002**, *67*, 2659–2664. Copyright 2002, American Chemical Society).

This is due to the fact that when the nitrogen of the Me_2N moiety becomes pyramidal at low temperature this moiety behaves similarly to an isopropyl group, which displays diastereotopic methyl groups in the presence of a chiral centre.[93] Line shape simulation provided N-inversion barriers of 11.3 and 9.3 kcal mol^{-1} for **48** and **49**, respectively.

Examples of molecules exhibiting both ring inversion and rotation have been reported for the six-membered cyclic compounds shown in Scheme 11.

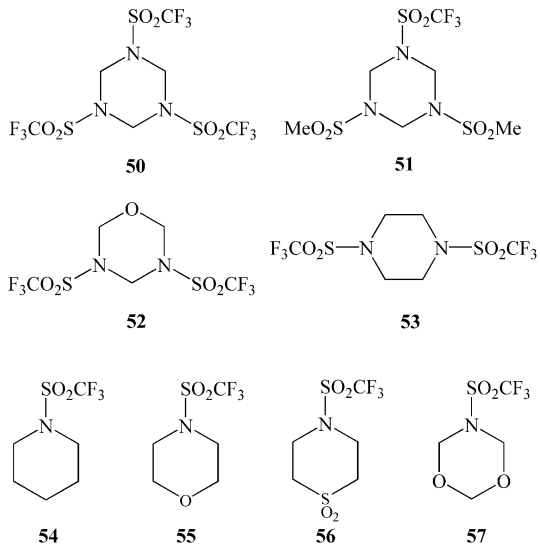

50 **51** **52** **53** **54** **55** **56** **57**

Scheme 11.

Compounds **50**–**57** have essentially planar nitrogen atoms, so the effects of N-inversion cannot be observed. On the other hand they all undergo ring inversion and N–S bond rotation processes that have been monitored by low-temperature ^1H, ^{13}C and ^{19}F spectroscopy.

At low temperature compound **50** exhibits a ring inversion process with a barrier ($\Delta G^{\neq}$) of 13.5 kcal mol^{-1} between two degenerate C_3 forms and a S–N bond rotation process between two unequally populated conformers ($\Delta G^{\neq}$ = 13.0 kcal mol^{-1}), the more stable having C_s symmetry and the less stable C_{3v} symmetry.[111]

When the three sulfonyl substituents are not identical, as in the case of **51**, DFT calculations predict that the compound can exist in three forms, due to the restricted N-inversion and N–S bond rotation. Two of these are sufficiently populated to be experimentally observed with a 6:1 relative proportion, the major having C_s symmetry and the minor C_1 symmetry. For both processes equal values of the barriers were estimated ($\Delta G^{\neq}$ = 13.5 kcal mol^{-1}).[112]

Compound **52** bears only two sulfonyl groups; restricted ring inversion together with N–S bond rotation give rise to two unequally populated conformers (ratio 7:1 in acetone), as observed by low-temperature ^1H NMR spectroscopy.[113] In CD_3OD at –80 °C the ^{19}F spectra showed two conformers with a 8.7:1 intensity ratio, the major having C_1 symmetry and the minor C_s symmetry, consistently with calculations predicting an energy difference of 0.81 kcal mol^{-1}. In contrast, X-ray diffraction indicates that only the minor conformer is present in the crystal. DFT computations predict an interconversion barrier of 11.7 kcal mol^{-1} corresponding to the N–S bond rotation, consistently with the experimentally estimated value of 11.5 kcal mol^{-1}.

Compound **53** exists as a mixture of three conformers (ratio 3:28:69), whereas compounds **54**–**56** each exist as a mixture of two conformers as a result of restricted ring inversion and N–S bond rotation.[114] The structural assignment was carried out by means of DFT computations. Be-

cause the interconversion barriers due to N–S bond rotation were not determined in the original paper the authors of this review have determined, by line shape simulation, a sample value in the case of compound **54** ($\Delta G^{\neq}$ = 9.0 ± 0.2 kcal mol^{-1}) by making use of the ^{19}F experimental spectra reported in Figure 1 (b) in the original article (see Figure S-23 in the Supporting Information).

In the case of compound **57** two chair conformers, corresponding to different arrangements of the SO_2CF_3 group, are present at –80 °C (ratio 84:16).[115] Computations indicate that a ring inversion pathway with intermediate formation of the corresponding 2,5-twist conformer has a calculated barrier (11.2 kcal mol^{-1}) in reasonable agreement with the experimentally estimated value of 11.7 kcal mol^{-1}.

Supporting Information (see also the footnote on the first page of this article): Figures S-1 to S-23 contain additional data (NMR and CD spectra, DFT calculated and X-ray diffraction structures) relating to compounds **8a**, **8b**, **10a**, **11a**, **12**, **19**, **20**, **26**, **28**, **30**, **36**, **37**, **44**–**47** and **54**.

Acknowledgments

The authors are indebted to the former Ph.D. students S. Davalli, M. A. Cremonini, R. Borghi, S. Grilli, C. Coluccini, M. Minzoni, and M. Mancinelli for their contributions during the last fifteen years.

[1] a) W. E. Stewart, T. H. Siddall III, *Chem. Rev.* **1970**, *70*, 517–551; b) E. L. Eliel, in: *Conformational Behavior of Six-Membered Rings. Analysis, Dynamics and Stereoelectronic Effects* (Ed.: E. Juaristi), chapter 1, pp. 1–24, VCH Publishers, New York, Weinheim, Cambridge, **1995**. See also ref.[4], ref.[6] (p. 575), ref.[15a,73,75,78,103,105] below.
[2] F. A. Bovey, *Nuclear Magnetic Resonance Spectroscopy*, chapter 7, pp. 183–210, Academic Press, New York, London, **1969**.
[3] H. Kessler, *Angew. Chem. Int. Ed. Engl.* **1970**, *9*, 219–235.
[4] F. A. L. Anet, R. Anet, in: *Determination of Organic Structure by Physical Methods* (Eds: F. C. Nachod, J. J. Zuckerman), vol. 3, chapter 7, pp. 344–420, Academic Press, New York, London, **1971**.
[5] J. B. Lambert, in: *Topics in Stereochemistry* (Eds: N. L. Allinger, E. L. Eliel), vol. 6, pp. 19–105, Wiley, New York, **1971**.
[6] *Dynamic Nuclear Magnetic Resonance Spectroscopy* (Eds: L. M. Jackman, F. A. Cotton), Academic Press, New York, London, **1975**.
[7] B. E. Mann, *Prog. NMR Spectrosc.* **1977**, *11*, 95–114.
[8] C. H. Bushweller, in: *Stereodynamics of Molecular Systems* (Ed.: R. H. Sharma), pp. 39–51, Pergamon Press, New York, Oxford, **1979**.
[9] J. Sandström, *Dynamic NMR Spectroscopy*, Academic Press London, New York, **1982**.
[10] M. Oki, *Applications of Dynamic NMR Spectroscopy to Organic Chemistry*, VCH Publishers Inc., Deerfield Beach, Florida, **1985**.
[11] *Acyclic Organonitrogen Stereodynamics* (Eds.: J. B. Lambert, Y. Takeuchi), VCH Publishers Inc., New York, Weinheim, Cambridge, **1992**.
[12] *Cyclic Organonitrogen Stereodynamics* (Eds.: J. B. Lambert, Y. Takeuchi), VCH Publishers Inc., New York, Weinheim, Cambridge, **1992**.
[13] C. H. Bushweller, in: *Conformational Behavior of Six-Membered Rings. Analysis, Dynamics and Stereoelectronic Effects* (Ed.: E. Juaristi), chapter 2, pp. 25–58, VCH Publishers, New York, Weinheim, Cambridge, **1995**.
[14] E. Kleinpeter, in: *Conformational Behavior of Six-Membered Rings. Analysis, Dynamics and Stereoelectronic Effects* (Ed.: E. Juaristi), chapter 6, pp. 201–243, VCH Publishers, New York, Weinheim, Cambridge, **1995**; E. Kleinpeter, in: *Advances in Heterocyclic Chemistry* (Ed.: A. Katritzky), vol. 69, chapter 4, pp. 217–269, Elsevier, Amsterdam, **1996**; E. Kleinpeter, in: *Advances in Heterocyclic Chemistry* (Ed.: A. Katritzky), vol. 86, chapter 2, pp. 41–126, Elsevier, Amsterdam, **1996**.
[15] a) L. Lunazzi, D. Macciantelli, A. Boicelli, *Tetrahedron Lett.* **1975**, *16*, 1205–1206; b) L. Lunazzi, D. Magagnoli, M. Guerra, D. Macciantelli, *Tetrahedron Lett.* **1979**, *20*, 3031–3032; c) L. Lunazzi, D. Macciantelli, G. Placucci, *Tetrahedron Lett.* **1980**, *21*, 975–976.
[16] C. H. Bushweller, J. W. O'Neil, *J. Am. Chem. Soc.* **1970**, *92*, 2159–2160.
[17] a) R. Ritter, W. Hull, H.-J. Cantow, *Tetrahedron Lett.* **1978**, *19*, 3093–3096; b) D. M. Pawar, J. Brown II, K.-H. Chen, N. L. Allinger, E. A. Noe, *J. Org. Chem.* **2006**, *71*, 6512–6515; c) J. Brown II, D. M. Pawar, E. A. Noe, *J. Org. Chem.* **2003**, *68*, 3420–3424; d) D. M. Pawar, S. D. Miggins, S. V. Smith, E. A. Noe, *J. Org. Chem.* **1999**, *64*, 2418–2421.
[18] D. M. Pawar, E. A. Noe, *J. Am. Chem. Soc.* **1998**, *120*, 5312–5314.
[19] NMR samples for examination at very low temperature should in any case be made more diluted than usual in order to reduce the risk of precipitation of the solute. At temperatures significantly lower than –100 °C the sensitivity is increased, however, because the volume of the solvent is reduced (so a larger number of nuclei is present within the RF coils) and, in addition, the excess population in the lower nuclear spin energy level is increased. In the case of quaternary carbon signals there is a further increase in sensitivity due to the fact that under these conditions the relaxation times become shorter (i.e., almost equal to those of the CH, CH_2 and CH_3 carbon signals).
[20] J. S. Siegel, F. A. L. Anet, *J. Org. Chem.* **1988**, *53*, 2629–2630.
[21] Recent international agreements on environmental concerns mean that some halogenated hydrocarbons of the Freon® type are no longer available commercially.
[22] F. A. L. Anet, I. Yavari, *J. Am. Chem. Soc.* **1977**, *99*, 6752–6753.
[23] F. A. L. Anet, G. Chmurny, J. Krane, *J. Am. Chem. Soc.* **1973**, *95*, 4423–4424.
[24] D. M. Pawar, E. A. Noe, *J. Org. Chem.* **1998**, *63*, 2850–2853.
[25] D. M. Pawar, E. A. Noe, *J. Am. Chem. Soc.* **1998**, *120*, 1485–1488.
[26] D. M. Pawar, K. K. Wilson, E. A. Noe, *J. Org. Chem.* **2000**, *65*, 1552–1553.
[27] W. D. Hounshell, L. D. Iroff, R. J. Wroczynski, K. Mislow, *J. Am. Chem. Soc.* **1978**, *100*, 5212–5213.
[28] D. Casarini, E. Foresti, L. Lunazzi, A. Mazzanti, *Chem. Eur. J.* **1999**, *5*, 3501–3508.
[29] T. Drakenberg, R. Jost, J. Sommer, *J. Chem. Soc., Chem. Commun.* **1974**, 1011–1012.
[30] F. A. L. Anet, I. Yavari, *J. Am. Chem. Soc.* **1977**, *99*, 2794–2796.
[31] F. A. L. Anet, A. K. Cheng, J. Krane, *J. Am. Chem. Soc.* **1973**, *95*, 7877–7878.
[32] H. J. Reich, W. H. Sikorski, A. W. Sanders, A. C. Jones, K. N. Plessel, *J. Org. Chem.* **2009**, *74*, 719–729.
[33] R. Annunziata, M. Benaglia, F. Cozzi, A. Mazzanti, *Chem. Eur. J.* **2009**, *15*, 4373–4381.
[34] F. A. L. Anet, A. K. Cheng, J. J. Wagner, *J. Am. Chem. Soc.* **1972**, *94*, 9250–9252.
[35] F. A. L. Anet, A. K. Cheng, *J. Am. Chem. Soc.* **1975**, *97*, 2420–2424.
[36] T. Olsson, D. Tanner, B. Thulin, O. Wennerström, T. Liljefors, *Tetrahedron* **1981**, *37*, 3473–3483.
[37] B. F. Bonini, L. Grossi, L. Lunazzi, D. Macciantelli, *J. Org. Chem.* **1986**, *51*, 517–522.

[38] We have found that the digital thermometer C9001 and thermocouple KX2384 (Comark Ltd., Hertfordshire, UK) are very reliable.
[39] D. A. Kleiner, G. Binsch, Program DNMR3, *QCPE 0165*, **1969**; J. H. Reich, *WinDNMR: Dynamic NMR Spectra for Windows®*, *J. Chem. Educ. Software* 3D2, **1996**; J. H. Brown, C. H. Bushweller, *QCPE* Program No. 633, **1993**; for a PC-based program to plot DNMR spectra, see: J. H. Brown, *QCPE* Program No. QCMP 123, **1993**. An interactive Windows®-based version of the QCPE 633 program is also available from the authors of this review.
[40] L. Lunazzi, A. Mazzanti, M. Minzoni, *J. Org. Chem.* **2005**, *70*, 10062–10066.
[41] E. J. Baerends, in the preface to: *A Chemist's Guide to Density Functional Theory*; see ref.[51]
[42] N. L. Allinger, Y. H. Yuh, J.-H. Lii, *J. Am. Chem. Soc.* **1989**, *111*, 8551–8566.
[43] *PCMODEL*, v9, Serena Software, Bloomington, IN (USA).
[44] T. A. Halgren, *J. Comput. Chem.* **1996**, *17*, 520–552.
[45] S. J. Weiner, P. A. Kollman, D. A. Case, U. C. Singh, C. Ghio, G. Alagona, S. Profeta, P. Weiner, *J. Am. Chem. Soc.* **1984**, *106*, 765–784.
[46] M. J. S. Dewar, E. G. Zoebisch, E. F. Healy, J. J. P. Stewart, *J. Am. Chem. Soc.* **1985**, *107*, 3902–3909.
[47] J. J. P. Stewart, *J. Comput. Chem.* **1989**, *10*, 209–220; J. J. P. Stewart, *J. Comput. Chem.* **1989**, *10*, 221–264.
[48] R. C. Bingham, M. J. S. Dewar, D. H. Lo, *J. Am. Chem. Soc.* **1975**, *97*, 1285–1293.
[49] The definition of "supercomputer" strongly depends upon the year of production.
[50] M. J. Frisch, M. Head-Gordon, J. A. Pople, *Chem. Phys. Lett.* **1990**, *166*, 281–289.
[51] W. Koch, M. C. Holthausen, *A Chemist's Guide to Density Functional Theory*, Wiley-VCH, Weinheim, 2nd ed., **2002**; *A Primer in Density Functional Theory* (Eds.: C. Fiolhais, F. Nogueira, M. Marques), Springer-Verlag, Heidelberg, **2003**.
[52] At the time of this review, a 3 GHz 16-core server could be acquired for about € 5000.
[53] M. J. Frisch, G. W. Trucks, H. B. Schlegel, G. E. Scuseria, M. A. Robb, J. R. Cheeseman, J. A. Montgomery, T. Vreven, K. N. Kudin, J. C. Burant, J. M. Millam, S. S. Iyengar, J. Tomasi, V. Barone, B. Mennucci, M. Cossi, G. Scalmani, N. Rega, G. A. Petersson, H. Nakatsuji, M. Hada, M. Ehara, K. Toyota, R. Fukuda, J. Hasegawa, M. Ishida, T. Nakajima, Y. Honda, O. Kitao, H. Nakai, M. Klene, X. Li, J. E. Knox, H. P. Hratchian, J. B. Cross, V. Bakken, C. Adamo, J. Jaramillo, R. Gomperts, R. E. Stratmann, O. Yazyev, A. J. Austin, R. Cammi, C. Pomelli, J. W. Ochterski, P. Y. Ayala, K. Morokuma, G. A. Voth, P. Salvador, J. J. Dannenberg, V. G. Zakrzewski, S. Dapprich, A. D. Daniels, M. C. Strain, O. Farkas, D. K. Malick, A. D. Rabuck, K. Raghavachari, J. B. Foresman, J. V. Ortiz, Q. Cui, A. G. Baboul, S. Clifford, J. Cioslowski, B. B. Stefanov, G. Liu, A. Liashenko, P. Piskorz, I. Komaromi, R. L. Martin, D. J. Fox, T. Keith, M. A. Al-Laham, C. Y. Peng, A. Nanayakkara, M. Challacombe, P. M. W. Gill, B. Johnson, W. Chen, M. W. Wong, C. Gonzalez, J. A. Pople, *Gaussian 03*, Gaussian Inc., Wallingford CT, **2004**.
[54] R. Ahlrichs, M. Bär, M. Häser, H. Horn, C. Kölmel, *Chem. Phys. Lett.* **1989**, *162*, 165–169; see also: http://www.turbomole.com/.
[55] *Spartan 08*, Wavefunction Inc., Irvine, CA (USA).
[56] R. A. Kendall, E. Apra, D. E. Bernholdt, E. J. Bylaska, M. Dupuis, G. I. Fann, R. J. Harrison, J. Ju, J. A. Nichols, J. Nieplocha, T. P. Straatsma, T. L. Windus, A. T. Wong, *Computer Phys. Commun.* **2000**, *128*, 260–283. See also: http://www.emsl.pnl.gov/capabilities/computing/nwchem/.
[57] a) C. E. Check, T. M. Gilbert, *J. Org. Chem.* **2005**, *70*, 9828–9834; b) M. D. Wodrich, C. Corminboeuf, P. v. R. Schleyer, *Org. Lett.* **2006**, *8*, 3631–3634; c) P. R. Shreiner, A. A. Fokin, R. A. Pascal, A. De Mejere, *Org. Lett.* **2006**, *8*, 3635–3638; d) S. Grimme, *Angew. Chem. Int. Ed.* **2006**, *45*, 4460–4464; e) Y. Zhao, D. G. Truhlar, *Org. Lett.* **2006**, *8*, 5753–5755; f) T. A. Rokob, A. Hamza, I. Pápai, *Org. Lett.* **2007**, *9*, 4279–4282; g) P. R. Shreiner, *Angew. Chem. Int. Ed.* **2007**, *46*, 4217–4219; h) M. D. Wodrich, C. S. Wannere, Y. Mo, P. D. Jarowski, K. N. Houk, P. v. R. Schleyer, *Chem. Eur. J.* **2007**, *13*, 7731–7744; i) Y. Zhao, D. G. Truhlar, *Acc. Chem. Res.* **2008**, *41*, 157–167; j) T. Schwabe, S. Grimme, *Acc. Chem. Res.* **2008**, *41*, 569–579; k) M. D. Wodrich, D. F. Jana, P. v. R. Schleyer, C. Corminboeuf, *J. Phys. Chem. A* **2008**, *112*, 11495–11500.
[58] A. D. Becke, *J. Chem. Phys.* **1993**, *98*, 5648–5652; C. Lee, W. Yang, R. G. Parr, *Phys. Rev. B* **1988**, *37*, 785–789; P. J. Stephens, F. J. Devlin, C. F. Chabalowski, M. J. Frisch, *J. Phys. Chem.* **1994**, *98*, 11623–11627.
[59] D. Young, in: *Computational Chemistry*, chapter 17, pp. 147–158, Wiley Interscience, New York, **2001**.
[60] Gaussview 4.1.2, Gaussian Inc., Wallingford CT, USA.
[61] *MOLDEN 4.6*, available at http://www.cmbi.ru.nl/molden/, see: G. Schaftenaar, J. H. Noordik, *J. Cold Reg. Eng. J. Comput. Aided Mol. Design* **2000**, *14*, 123–134; *Chem. Abstr.* **2000**, *132*, 321509.
[62] C. F. Tormena, R. Rittner, R. J. Abraham, E. A. Basso, B. C. Fiorin, *J. Phys. Org. Chem.* **2004**, *17*, 42–48.
[63] M. W. Wong, *Chem. Phys. Lett.* **1996**, *256*, 391–399.
[64] R. Ruzziconi, S. Spizzichino, L. Lunazzi, A. Mazzanti, M. Schlosser, *Chem. Eur. J.* **2009**, *15*, 2645–2652.
[65] G. Bifulco, P. Dambruoso, L. Gomez-Paloma, R. Riccio, *Chem. Rev.* **2007**, *107*, 3744–3779; A. Bagno, G. Saielli, *Theor. Chem. Acc.* **2007**, *117*, 603–619.
[66] D. M. Pawar, E. A. Noe, *J. Am. Chem. Soc.* **1996**, *118*, 12821–12825.
[67] D. Casarini, L. Lunazzi, A. Mazzanti, G. Simon, *J. Org. Chem.* **2000**, *65*, 3207–3208.
[68] D. M. Pawar, K. L. Davis, B. L. Brown, S. V. Smith, E. A. Noe, *J. Org. Chem.* **1999**, *64*, 4580–4585.
[69] G. Bringmann, A. J. Price Mortimer, P. A. Keller, M. J. Gresser, J. Garner, M. Breuning, *Angew. Chem. Int. Ed.* **2005**, *44*, 5384–5427.
[70] a) R. L. Clough, J. D. Roberts, *J. Am. Chem. Soc.* **1976**, *98*, 1018–1020; b) R. Cosmo, S. Sternhell, *Aust. J. Chem.* **1987**, *40*, 1107–1126; c) F. Cozzi, M. Cinquini, R. Annunziata, J. S. Siegel, *J. Am. Chem. Soc.* **1993**, *115*, 5330–5331; d) S. Lavieri, J. A. Zoltewicz, *J. Org. Chem.* **2001**, *66*, 7227–7230; e) G. E. Tumambac, C. Wolf, *J. Org. Chem.* **2005**, *70*, 2930–2938.
[71] C. Dell'Erba, F. Gasparrini, S. Grilli, L. Lunazzi, A. Mazzanti, M. Novi, M. Pierini, C. Tavani, C. Villani, *J. Org. Chem.* **2002**, *67*, 1663–1668.
[72] S. Grilli, L. Lunazzi, A. Mazzanti, M. Pinamonti, *Tetrahedron* **2004**, *60*, 4451–4458.
[73] L. Lunazzi, M. Mancinelli, A. Mazzanti, *J. Org. Chem.* **2007**, *72*, 5391–5394.
[74] a) H. O. House, J. A. Hrabie, D. VanDerveer, *J. Org. Chem.* **1986**, *51*, 921–929; b) H. O. House, J. T. Holt, D. VanDerveer, *J. Org. Chem.* **1993**, *58*, 7516–7523.
[75] a) A. Dondoni, L. Lunazzi, P. Giorgianni, D. Macciantelli, *J. Org. Chem.* **1975**, *40*, 2979–2980; b) S. Hoogasian, C. H. Bushweller, W. G. Anderson, G. Kigsley, *J. Phys. Chem.* **1976**, *80*, 643–648; c) L. Lunazzi, G. Cerioni, K. U. Ingold, *J. Am. Chem. Soc.* **1976**, *98*, 7484–7488; d) L. Lunazzi, A. Dondoni, G. Barbaro, D. Macciantelli, *Tetrahedron Lett.* **1977**, *18*, 1079–1080; e) L. Forlani, L. Lunazzi, A. Medici, *Tetrahedron Lett.* **1977**, *18*, 4525–4526; f) F. Bernardi, L. Lunazzi, P. Zanirato, G. Cerioni, *Tetrahedron* **1977**, *33*, 1337–1343; g) L. Lunazzi, C. Magagnoli, M. Guerra, D. Macciantelli, *Tetrahedron Lett.* **1979**, *20*, 3031–3032; h) M. A. Cremonini, L. Lunazzi, G. Placucci, R. Okazaki, G. Yamamoto, *J. Am. Chem. Soc.* **1990**, *112*, 2915–2921; i) L. Lunazzi, D. Macciantelli, L. Grossi, *Tetrahedron* **1983**, *39*, 305–308; j) J. E. Anderson, D. A. Tocher, D. Casarini, L. Lunazzi, *J. Org. Chem.* **1991**, *56*, 1731–1739; k) R. Borghi, L. Lunazzi, G. Placucci, G. Cerioni, E. Foresti, A.

Plumitallo, *J. Org. Chem.* **1997**, *62*, 4924–4927; l) M. B. Garcia, S. Grilli, L. Lunazzi, A. Mazzanti, L. R. Orelli, *J. Org. Chem.* **2001**, *66*, 6679–6684; m) M. B. Garcia, S. Grilli, L. Lunazzi, A. Mazzanti, L. R. Orelli, *Eur. J. Org. Chem.* **2002**, 4018–4023; n) D. Casarini, C. Rosini, S. Grilli, L. Lunazzi, A. Mazzanti, *J. Org. Chem.* **2003**, *68*, 1815–1820; o) D. Casarini, S. Grilli, L. Lunazzi, A. Mazzanti, *J. Org. Chem.* **2004**, *69*, 345–351; p) G. Bartoli, L. Lunazzi, M. Massacesi, A. Mazzanti, *J. Org. Chem.* **2004**, *69*, 821–825; q) D. Casarini, C. Coluccini, L. Lunazzi, A. Mazzanti, R. Rompietti, *J. Org. Chem.* **2004**, *69*, 5746–5748.

[76] L. Lunazzi, A. Mazzanti, *J. Am. Chem. Soc.* **2004**, *126*, 12155–12157.

[77] L. Lunazzi, M. Mancinelli, A. Mazzanti, *J. Org. Chem.* **2008**, *73*, 2198–2205.

[78] L. Lunazzi, M. Mancinelli, A. Mazzanti, *J. Org. Chem.* **2007**, *72*, 10045–10050.

[79] The use of the TD-DFT method for the determination of the absolute configurations of organic compounds has recently been reviewed, see: G. Bringmann, T. Bruhn, K. Maksimenka, Y. Hemberger, *Eur. J. Org. Chem.* **2009**, 2717–2727.

[80] J. E. Anderson, D. Casarini, L. Lunazzi, *Tetrahedron Lett.* **1988**, *29*, 3141–3144.

[81] a) F. Grein, *J. Phys. Chem. A* **2002**, *106*, 3823–3827; b) M. P. Johansson, J. Olsen, *J. Chem. Theory Comput.* **2008**, *4*, 1460–1471.

[82] L. Lunazzi, M. Mancinelli, A. Mazzanti, *J. Org. Chem.* **2008**, *73*, 5354–5359.

[83] L. Lunazzi, M. Mancinelli, A. Mazzanti, *J. Org. Chem.* **2009**, *74*, 1345–1348.

[84] J. E. Anderson, A. de Meijere, S. I. Kozhushkov, L. Lunazzi, A. Mazzanti, *J. Am. Chem. Soc.* **2002**, *124*, 6706–6713.

[85] S. Grilli, L. Lunazzi, A. Mazzanti, M. Pinamonti, J. E. Anderson, C. V. Ramana, P. S. Koranne, M. K. Gurjar, *J. Org. Chem.* **2002**, *67*, 6387–6394.

[86] R. W. Alder, P. R. Allen, K. R. Anderson, C. P. Butts, E. Khosravi, A. Martin, C. M. Maunder, A. G. Orpen, C. B. St. Pourçain, *J. Chem. Soc. Perkin Trans. 2* **1998**, 2083–2107.

[87] R. W. Alder, P. R. Allen, D. Hnyk, D. W. H. Rankin, H. E. Robertson, B. A. Smart, R. J. Gillespie, I. Bytheway, *J. Org. Chem.* **1999**, *64*, 4226–4232.

[88] C. V. Ramana, S. M. Baquer, R. G. Gonnade, M. K. Gurjar, *Chem. Commun.* **2002**, 614–615.

[89] a) G. P. Newsoroff, S. Sternhell, *Tetrahedron Lett.* **1967**, *8*, 2539–2542; b) J. M. A. Baas, A. Sinnema, *Recl. Trav. Chim. Pays-Bas* **1973**, *92*, 899–905; c) J. M. A. Baas, J. M. van der Toorn, B. M. Wepster, *Recl. Trav. Chim. Pays-Bas* **1974**, *93*, 133–135; d) D. Landman, G. P. Newsoroff, S. Sternhell, *Aust. J. Chem.* **1972**, *25*, 109–128; e) H. Suezawa, H. Wada, H. Watanabe, T. Yuzuri, K. Sakakibara, M. Hirota, *J. Phys. Org. Chem.* **1997**, *10*, 925–934; f) S. Andersson, T. Drakenberg, *Org. Magn. Reson.* **1983**, *21*, 730–744; g) J. S. Lomas, J.-E. Dubois, *J. Org. Chem.* **1976**, *41*, 3033–3034; h) J. S. Lomas, P. K. Luong, J.-E. Dubois, *J. Org. Chem.* **1977**, *42*, 3394–3399; i) J. S. Lomas, J.-E. Dubois, *Tetrahedron* **1981**, *37*, 2273–2278; j) J. S. Lomas, J. Vaissermann, *J. Chem. Soc. Perkin Trans. 2* **1998**, 1777–1781; k) J. S. Lomas, *J. Chem. Soc. Perkin Trans. 2* **2001**, 754–757; l) J. S. Lomas, A. Adenier, *J. Chem. Soc. Perkin Trans. 2* **2002**, 1264–1270; m) J. E. Anderson, V. Bru-Capdeville, P. A. Kirsch, J. S. Lomas, *J. Chem. Soc., Chem. Commun.* **1994**, 1077–1078; n) J. S. Lomas, J. E. Anderson, *J. Org. Chem.* **1995**, *60*, 3246–3248; o) D. Casarini, L. Lunazzi, A. Mazzanti, *J. Org. Chem.* **1997**, *62*, 3315–3323; p) C. Wolf, L. Pranatharthiaran, R. B. Ramagosa, *Tetrahedron Lett.* **2002**, *43*, 8563–8567.

[90] a) L. E. Eliel, S. H. Wilen, *Stereochemistry of Organic Compounds*, p. 21, John Wiley & Sons, New York, **1994**; b) C. Wolf, *Dynamic Stereochemistry of Chiral Compounds*, p. 500, RSC Publishing, Cambridge, **2008**.

[91] D. Casarini, C. Coluccini, L. Lunazzi, A. Mazzanti, *J. Org. Chem.* **2005**, *70*, 5098–5102.

[92] D. Casarini, C. Coluccini, L. Lunazzi, A. Mazzanti, *J. Org. Chem.* **2006**, *71*, 4490–4496.

[93] K. Mislow, M. Raban, *Top. Stereochem.* **1967**, *1*, 1; W. B. Jennings, *Chem. Rev.* **1975**, *75*, 307–322; E. L. Eliel, *J. Chem. Educ.* **1980**, *57*, 52.

[94] D. Casarini, C. Rosini, S. Grilli, L. Lunazzi, A. Mazzanti, *J. Org. Chem.* **2003**, *68*, 1815–1820.

[95] For a treatment of the exciton model and its applications to organic stereochemistry, see: a) S. F. Mason, *Quart. Rev.* **1963**, *17*, 20–66; b) S. F. Mason, in: *Optical Rotatory Dispersion and Circular Dichroism in Organic Chemistry* (Ed.: G. Snatzke), chapter 4, p. 71, Wiley, London, **1967**; c) N. Harada, K. Nakanishi, *Acc. Chem. Res.* **1972**, *5*, 257–263; d) N. Harada, K. Nakanishi, *Circular Dichroic Spectroscopy: Exciton Coupling in Organic Stereochemistry*; University Science Books, Mill Valley, CA, **1983**; e) K. Nakanishi, N. Berova, in: *Circular Dichroism: Principle and Applications* (Eds.: N. Berova, K. Nakanishi, R. W. Woody), chapter 12, p. 337, VCH, New York, **2000**.

[96] D. Casarini, S. Grilli, L. Lunazzi, A. Mazzanti, *J. Org. Chem.* **2004**, *69*, 345–351.

[97] S. Toyota, T. Makino, *Tetrahedron Lett.* **2003**, *44*, 7775–7778.

[98] C. H. Bushweller, in: *Acyclic Organonitrogen Stereodynamics* (Eds.: J. B. Lambert, Y. Takeuchi), pp. 1–35, VCH Publishers, New York, Weinheim, Cambridge **1992**.

[99] M. Raban, D. Kost, in: *Acyclic Organonitrogen Stereodynamics* (Eds.: J. B. Lambert, Y. Takeuchi), pp. 37–88, VCH Publishers, New York, Weinheim, Cambridge **1992**.

[100] S. F. Nelsen, in: *Acyclic Organonitrogen Stereodynamics* (Eds.: J. B. Lambert, Y. Takeuchi), pp. 89–121, VCH Publishers, New York, Weinheim, Cambridge **1992**.

[101] J. H. Brown, C. H. Bushweller, *J. Org. Chem.* **2001**, *66*, 903–909.

[102] A two-letter designation has been used to name conformations. The first letter defines the orientation of the propargyl quaternary carbon (**G** denotes *gauche* to the lone pair and to the *N*-methyl group; **G′** denotes *gauche* to the lone pair and to the isopropyl group; **A** denotes *anti* to the lone pair). The second letter defines the orientation of the isopropyl methine proton (**G** denotes *gauche* to the lone pair and to the *N*-methyl group; **G′** denotes *gauche* to the lone pair and to the propargyl group; **A** denotes *anti* to the lone pair).

[103] J. G. Jewett, J. J. Breeyear, J. H. Brown, C. H. Bushweller, *J. Am. Chem. Soc.* **2000**, *122*, 308–323. For a similar compound see: J. E. Anderson, D. Casarini, A. I. Ijeh, L. Lunazzi, D. A. Tocher, *J. Am. Chem. Soc.* **1995**, *117*, 3054–3056.

[104] Other cases in which a barrier cannot be observed until the lower barrier is frozen have been reported: a) W. R. Jackson, W. B. Jennings, *Tetrahedron Lett.* **1974**, *15*, 1837–1838; b) J. E. Anderson, D. Casarini, A. J. Ijeh, L. Lunazzi, *J. Am. Chem. Soc.* **1997**, *119*, 8050–8057; c) D. Casarini, L. Lunazzi, A. Mazzanti, E. Foresti, *J. Org. Chem.* **1998**, *63*, 4746–4754; d) L. Lunazzi, A. Mazzanti, A. Muñoz Álvarez, *J. Org. Chem.* **2000**, *65*, 3200–3206.

[105] O. Lukoyanova, A. Kitaygorodskiy, C. M. Cardona, L. Echegoyen, *Chem. Eur. J.* **2007**, *13*, 8294–8301.

[106] D. Eisenberg, A. S. Filatov, E. A. Jackson, M. Rabinovitz, M. A. Petrukhina, L. T. Scott, R. Shenhar, *J. Org. Chem.* **2008**, *73*, 6073–6078.

[107] The probe was $HOCMe_2$, as in: L. T. Scott, M. M. Hashemi, M. S. Bratcher, *J. Am. Chem. Soc.* **1992**, *114*, 1920–1921.

[108] Y. Wang, A. D. Stretton, M. C. McConnell, P. A. Wood, S. Parsons, J. B. Henry, A. R. Mount, T. H. Galow, *J. Am. Chem. Soc.* **2007**, *129*, 13193–13200.

[109] G. Schwab, D. Stern, D. Stalke, *J. Org. Chem.* **2008**, *73*, 5242–5247.

[110] G. Bartoli, S. Grilli, L. Lunazzi, M. Massaccesi, A. Mazzanti, S. Rinaldi, *J. Org. Chem.* **2002**, *67*, 2659–2664.

[111] B. A. Shainyan, V. I. Meshcheryakov, A. I. Albanov, M. V. Sigalov, *Tetrahedron Lett.* **2005**, *46*, 6199–6201.

[112] B. A. Shainyan, I. A. Ushakov, A. Koch, E. Kleinpeter, *J. Org. Chem.* **2006**, *71*, 7638–7642.
[113] B. A. Shainyan, I. A. Ushakov, V. I. Meshcheryakov, U. Schilde, A. Koch, E. Kleinpeter, *Tetrahedron* **2007**, *63*, 11828–11837.
[114] B. A. Shainyan, I. A. Ushakov, L. L. Tolstikova, A. Koch, E. Kleinpeter, *Tetrahedron* **2008**, *64*, 5208–5216.
[115] B. A. Shainyan, I. A. Ushakov, V. I. Meshcheryakov, A. Koch, E. Kleinpeter, *Tetrahedron* **2008**, *64*, 5379–5383.
Received: November 20, 2009
Published Online: February 19, 2010

